Title

GIGYF2 and 4EHP Inhibit Translation Initiation of Defective Messenger RNAs to Assist Ribosome-Associated Quality Control.

Journal

Molecular cell, 79(6)

ISSN

1097-2765

Authors

Hickey, Kelsey L
Dickson, Kimberley
Cogan, J Zachery
et al.

Publication Date

2020-09-01

DOI

10.1016/j.molcel.2020.07.007

Peer reviewed

Published in final edited form as:

Mol Cell. 2020 September 17; 79(6): 950–962.e6. doi:10.1016/j.molcel.2020.07.007.

GIGYF2 and 4EHP Inhibit Translation Initiation of Defective Messenger RNAs to Assist Ribosome-Associated Quality Control

Kelsey L. Hickey[1], **Kimberley Dickson**[2], **J. Zachery Cogan**[1], **Joseph M. Replogle**[1], **Michael Schoof**[6], **Karole N. D'Orazio**[3], **Niladri K. Sinha**[3], **Jeffrey A. Hussmann**[1,4], **Marco Jost**[1,4], **Adam Frost**[5,6,7], **Rachel Green**[3,8], **Jonathan S. Weissman**[1,5,8,*], **Kamena K. Kostova**[9,*]

[1]Department of Cellular and Molecular Pharmacology, University of California, San Francisco, San Francisco, CA 94158, USA

[2]Lawerence University, Department of Biology, Appleton, WI 54911, USA

[3]Johns Hopkins University, Department of Biology, Baltimore, MD, 21218, USA

[4]Department of Microbiology and Immunology, University of California, San Francisco, San Francisco, CA 94158, USA

[5]California Institute for Quantitative Biomedical Research, University of California, San Francisco, San Francisco, CA 94158, USA

[6]Department of Biochemistry and Biophysics, University of California, San Francisco, San Francisco, CA 94158, USA

[7]Chan Zuckerberg Biohub, San Francisco, CA 94158, USA

[8]Howard Hughes Medical Institute

[9]Carnegie Institution for Science, Department of Embryology, Baltimore, MD, 21218, USA

Summary

Ribosome-associated Quality Control (RQC) pathways protect cells from toxicity caused by incomplete protein products resulting from translation of damaged or problematic mRNAs. Extensive work in yeast has identified highly conserved mechanisms that lead to the degradation of the faulty mRNA and partially synthesized polypeptide. Here, we used CRISPR-Cas9-based screening to search for additional RQC strategies in mammals. We found that failed translation leads to specific inhibition of translation initiation on that message. This negative feedback loop is mediated by two translation inhibitors, GIGYF2 and 4EHP. Both model substrates and growth-based assays established that inhibition of additional rounds of translation acts in concert with known RQC pathways to prevent buildup of toxic proteins. Inability to block translation of faulty

*Corresponding authors. jonathan.weissman@ucsf.edu, Kostova@carnegiescience.edu.

Author Contributions:

K.K., K.D., K.L.H., A.F., and J.S.W. conceived the study. K.L.H., K.K. and J.S.W. wrote the manuscript with input from all authors. K.L.H., K.K., K.D., J.M.R, J.Z.C., M.S., K.N.D., and N.K.S. performed all experiments. M.J. contributed to genetic interaction experiments, M.J., J.A.H., and J.M.R. performed data analysis.

Declaration of Interests:

The authors declare no competing interests.

mRNAs, and subsequent accumulation of partially synthesized polypeptides, could explain the neurodevelopmental and neuropsychiatric disorders observed in mice and humans with compromised GIGYF2 function.

Introduction

Translation is an enormous amplification step in which each messenger RNA (mRNA) is turned into hundreds of proteins. Defective mRNAs lacking a stop codon due to premature polyadenylation or mRNAs harboring damage, non-optimal codons or RNA structure can cause ribosomes to stop translating before they reach a stop codon (Doma and Parker, 2006; Klauer and van Hoof, 2012; Letzring et al., 2013). Such stalled ribosomes pose numerous threats to the cells as they decrease protein output from an mRNA, block translation by trailing ribosomes, and carry incomplete polypeptide that can aggregate or exhibit dysregulated activity (Choe et al., 2016; Chu et al., 2009; Yonashiro et al., 2016). Therefore, if ribosome stalling is not detected and resolved, it can jeopardize cell and organismal viability.

To counter the threat posed by stalled ribosomes, cells possess multiple surveillance mechanisms, collectively referred to here as Ribosome-associated Quality Control (RQC) pathways. Recent studies have shown that one of the earliest events that can initiate the RQC is the collision between the stalled ribosome and a trailing one (Juszkiewicz and Hegde, 2017; Juszkiewicz et al., 2018; Simms et al., 2017; Sundaramoorthy et al., 2017). One mechanism of detection of such collided disomes is mediated by an E3 ubiquitin ligase Hel2p (ZNF598 in human) (Brandman et al., 2012; Garzia et al., 2017; Juszkiewicz et al., 2018; Letzring et al., 2013; Matsuo et al., 2017; Saito et al., 2015; Shao et al., 2015; Sundaramoorthy et al., 2017). After detection, the stalled ribosome is dissociated by the combined action of Dom34p/ Hbs1p (Izawa et al., 2012) and the RQC-Trigger complex (Hashimoto et al., 2020; Matsuo et al., 2017). The 60S ribosome, which still carries the stalled nascent polypeptide, recruits the core RQC components, allowing the nascent polypeptide to be ubiquitinated and extracted from the exit tunnel for proteasomal degradation (Bengtson and Joazeiro, 2010; Brandman et al., 2012; Kostova et al., 2017; Osuna et al., 2017).

These quality control pathways have been discovered and extensively studied in yeast. However, far less is known about their conserved counterparts in mammals. In contrast to yeast, where loss of core RQC factors is well tolerated under standard growth conditions, mutations in the mammalian factors affect cell growth and have been associated with complex disease. For example, partial loss-of-function mutations in LTN1, the ubiquitin ligase facilitating the degradation of the stalled nascent polypeptide, cause neurodegeneration in mice (Bengtson and Joazeiro, 2010; Chu et al., 2009). Together, these observations further emphasize the importance of RQC for maintaining protein homeostasis in higher eukaryotes (Brandman et al., 2012; Defenouillère et al., 2013; Shao and Hegde, 2014; Shao et al., 2013; Verma et al., 2013). Given the toxicity of partially synthesized proteins, it is possible that multiple layers of regulation exist to prevent, detect, and cope with ribosome stalling. However, our understanding of how the RQC cooperates with other

pathways governing protein homeostasis is incomplete. Here we use reporter-based and growth-based genome-wide CRISPRi screens (Gilbert et al., 2014; Qi et al., 2013) to systematically characterize the mammalian RQC pathway. We identify a new branch of the RQC that involves two factors, GIGYF2 and 4EHP, that block ribosome initiations on problematic mRNAs.

Results

CRISPRi screen for mammalian factors that promote accumulation of a Non-stop decay substrate.

To systematically explore how mammalian cells cope with problematic mRNAs, we designed a mammalian RQC reporter that contains an open-reading frame encoding for the green fluorescent protein, but no stop codon ($GFP_{Non\text{-}stop}$) (Fig. 1A). Since the encoded GFP lacks a stop codon, translation through the GFP to the end of the message (Fig. S1A) causes ribosome stalling and subsequent degradation of the GFP nascent polypeptide via the RQC pathway. Incomplete proteins generated from such messages are model substrates for RQC-mediated degradation in yeast (Bengtson and Joazeiro, 2010) but have not been studied in mammals. Upstream of the GFP, the reporter encodes BFP separated by a T2A ribosome skipping sequence (Fig. 1A). As a result, BFP synthesis is uncoupled from RQC-mediated degradation of GFP, allowing BFP to serve as control for the expression levels of the reporter. Since messages lacking a stop codon are rapidly degraded by the exosome (Frischmeyer et al., 2002) we introduced a triple helix derived from the MALAT1 non-coding RNA at the 3' end to stabilize the message (Wilusz et al., 2012). Wild type cells accumulate BFP, but not GFP, resulting in a substantial decrease (~ 100 fold) in the GFP/BFP ratio for the $GFP_{Non\text{-}stop}$ reporter compared to two control reporters that contain either a stop codon before the MALAT1 sequence (GFP_{Stop}), or a stop codon and a canonical polyA tail (GFP_{PolyA}) (Fig. 1A, B). Knockdown of a core RQC component, *NEMF* (*RQC2* in yeast), led to the stabilization of GFP (Fig. 1C, Fig. S1B), confirming the role of mammalian NEMF in degradation of nascent polypeptides resulting from non-stop decay mRNAs (Shao et al., 2015).

We next used the $GFP_{Non\text{-}stop}$ reporter in a fluorescence-activated cell sorting (FACS)-based genome-wide CRISPRi screen to gain a comprehensive view of mechanisms that cells have for minimizing the accumulation of nascent polypeptides resulting from mRNAs lacking a stop codon. We engineered a K562 mammalian cell line that constitutively expresses the $GFP_{Non\text{-}stop}$ reporter and the dCas9-KRAB CRISPRi effector (Gilbert et al., 2014) and transduced this cell line with an sgRNA library (hCRISPRi-v2) targeting all known protein-coding open reading frames (Horlbeck et al., 2016). We hypothesized that depletion of RQC factors will interfere with the ability of the cells to detect stalled ribosomes and degrade the stalled nascent polypeptide, which will result in GFP stabilization. We then sorted the cells with high and low GFP signal via FACS and identified the genes that were depleted in those cells by deep sequencing the sgRNAs they expressed. (Fig. 1D, E). The screen identified the majority of known components from each stage of the RQC pathway (stall detection, ribosome splitting, nascent chain extraction, mRNA and peptide degradation) as top hits

(Fig. 1E, F, S1C, D). In addition to factors previously implicated in the RQC pathway, the FACS-based screen yielded several genes with no known RQC-related function.

Genetic interaction screen identifies the translation inhibitors GIGYF2 and 4EHP as RQC components working in parallel to nascent polypeptide degradation by NEMF.

To differentiate between factors that allow mammalian cells to cope with stalled ribosomes as part of the RQC from components of parallel proteostasis pathways, we complemented our reporter-based screen with a growth-based CRISPRi genetic interaction (GI) screen. We aimed to search for components that have synergistic growth defects in combination with loss of NEMF. This idea was motivated in part by recent findings that combined loss of the NEMF homolog in bacteria (RqcH) and the tmRNA/ ssrA pathway, which helps dispose of incomplete translation products, leads to a synergistic growth defect. (Lytvynenko et al., 2019). To test whether similar pathways exist in combination with the mammalian RQC pathway, we took advantage of the growth defect caused by NEMF depletion (Fig. 2A). We engineered a cell line constitutively expressing a *NEMF*-targeting sgRNA, as well as a paired cell line constitutively expressing a non-targeting control sgRNA, and infected both cell lines with the genome-wide CRISPRi sgRNA library (Fig. 2B). We determined the change in the sgRNA abundance over 10 doublings for each cell lines and then compared this change between the two cell lines. We expected that depletion of RQC components will have similar effect on growth alone or in combination with *NEMF* knockdown (buffering interaction) (Fig. 2C). On the other hand, disruption of pathways that work in parallel with RQC to prevent the accumulation of failed translation products is expected to exacerbate the growth phenotype caused by loss of *NEMF* (synergistic interaction). Indeed, the screen revealed several factors that exhibit buffering or synergistic growth interactions with loss of NEMF (Fig. 2D).

We then compared the hits from the FACS-based reporter screen and the modifier screen. Two genes stood out as having both a strong synergistic interaction with loss of NEMF and stabilizing effect on the RQC reporter upon knockdown: *PATL1* and *GIGYF2* (Fig. 2E). *PATL1* encodes a scaffold protein that bridges mRNA decapping and deadenylation (Ozgur et al., 2010). Stabilization of damaged mRNAs in the absence of PATL1 could explain both the increased levels of stalled nascent polypeptides and the synergistic growth interaction with *NEMF* knockdown, which disposes of incomplete protein products from such damaged mRNAs. We focused our attention on the second gene, *GIGYF2*, which had not been previously implicated in the cellular response to damaged mRNAs.

Overexpression studies of tagged GIGYF2 have shown that it interacts with the inhibitory cap-binding protein 4EHP (Peter et al., 2017) and the ribosome collision sensor ZNF598 (Morita et al., 2012; Tollenaere et al., 2019). Indeed, 4EHP and ZNF598 co-immunoprecipitated with GIGYF2 endogenously tagged with GFP11, confirming that these three proteins interact in cells (Fig. 3A). In addition, GIGYF2 and 4EHP were strongly enriched upon immunoprecipitation of FLAG- tagged ZNF598, as quantified by mass spectrometry (Fig. S2A).

Although an interaction between GIGYF2 and ZNF598 has been reported, the role of GIGYF2 and 4EHP in ribosome-associated quality control has not been explored. Based on

our GI screen, knockdown of GIGYF2 or 4EHP in combination with knockdown of NEMF leads to a synergistic growth defect. This result suggests that GIGYF2 and 4EHP function in parallel to the RQC pathway to counter accumulation of toxic polypeptides resulting from ribosome stalling. We were able to recapitulate the GI screen results in targeted studies (Fig. 3B). The moderate growth phenotype imparted by knockdown of *NEMF* was exacerbated by *GIGYF2* knockdown (Fig. 3C). Similarly, *4EHP* knockdown also had a synergistic interaction with *NEMF* knockdown, suggesting that GIGYF2 and 4EHP work in parallel to NEMF. In addition, *ZNF598* knockdown had buffering interactions with GIGYF2 and 4EHP knockdown (Fig. 3D, Fig S2B, C) consistent with the data that these three proteins form a complex and work together in the same pathway.

GIGYF2, 4EHP, and ZNF598 inhibit translation of faulty mRNAs

4EHP (EIF4E2) is an ortholog of the mRNA cap-binding and translation initiation factor EIF4E1. However, 4EHP cannot bind EIF4G and as a result it blocks assembly of productive EIF4F initiation complex (Rom et al., 1998; Zuberek et al., 2007), thereby repressing translation of the bound mRNA. Indeed, recruitment of GIGYF2 or 4EHP to reporter messages has been shown to block translation initiation (Kryszke et al., 2016; Morita et al., 2012). It has been hypothesized that GIGYF2 requires an adapter protein for recruitment to its target mRNA, although the endogenous substrates and recruitment factors remain incompletely characterized. Our genetic and biochemical studies suggest a model in which ZNF598 could act as one such factor that recruits GIGYF2 and 4EHP to messages harboring stalled ribosomes, which ultimately leads to translational silencing of the mRNA. To test this model, we measured the effect of knocking down these proteins on the $GFP_{Non\text{-}stop}$ fluorescent reporter. We compared the levels of BFP, which is released before stalling and is, therefore, a readout of the reporter expression levels, and GFP, which is degraded due to ribosome stalling (Fig. 4A). As expected, knockdown of *NEMF*, a factor involved in the degradation of the stalled nascent polypeptide, increased GFP, but not BFP levels. Knockdown of *GIGYF2* or *4EHP,* however, increased the levels of both fluorescent proteins (Fig. 4A) without affecting reporter mRNA levels (Fig. 4B), or protein half-life (Fig. S2D) supporting the hypothesis that these two factors are translation inhibitors. Surprisingly, knockdown of *ZNF598* also increased both BFP and GFP levels, although to a lesser extent. This observation suggests that ZNF598 can also play a role in translational repression.

To directly measure the changes in ribosome occupancy on our $GFP_{Non\text{-}stop}$ stalling reporter, we performed ribosome profiling. Consistent with the fluorescent reporter assay, the translation efficiency (TE) of the reporter was increased in both GIGYF2 and 4EHP knockdown cell lines (Fig. 4C), with minimal changes in the reporter mRNA expression levels (Fig. S3A). When compared to endogenous messages with similar expression levels, the $GFP_{Non\text{-}stop}$ reporter has one of the highest TE changes upon loss of GIGYF2 (Fig. 4D, S3B). In addition, we find that the TE of endogenous messages is not affected by GIGYF2 or 4EHP knockdown, regardless of their expression levels (Fig. S3C, D). Taken together, these data support a model where GIGYF2/4EHP block translation on problematic messages.

To ensure that the observed translational effect was specific to faulty mRNAs, and not due to global changes in protein production, we used a second set of reporters with bidirectional promoters. One promoter drives expression of an mRNA coding for GFP with a canonical stop codon and polyA tail, and the other drives a non-stop reporter ($RFP_{Non\text{-}stop}$) or a control fluorescent protein (RFP_{Stop}) on a separate mRNA. Importantly, these cell lines have similar expression levels for the stalling and non-stalling reporters as confirmed by qPCR (Fig. S4A, B). Knockdown of *NEMF*, *GIGYF2*, and *4EHP* increased the RFP/GFP ratio for $RFP_{Non\text{-}stop}$, but not RFP_{Stop} (Fig. 4E). These knockdowns did not have a global effect on translation as the levels of the non-stalling controls were unchanged (Fig 4F, Fig. S4C – F). The observed $RFP_{Non\text{-}stop}$ stabilization was not due to changes in mRNA levels (Fig S4G), consistent with the $GFP_{Non\text{-}stop}$ reporter used in our original screen. In addition, a simultaneous knockdown of *NEMF* and *GIGYF2* increased the RFP/GFP ratio to a greater extent than either single knockdown, further suggesting that these factors are components of two parallel pathways coping with ribosome stalling.

We confirmed that the observed translational silencing does not depend on the type of stall by measuring the effect of *GIGYF2* and *4EHP* knockdown on a fluorescent reporter containing a previously characterized mammalian stalling sequence, 20 AAA (K20) (Juszkiewicz and Hegde, 2017). Similar to the $GFP_{Non\text{-}stop}$ reporter, knockdown of *GIGYF2* or *4EHP* led to an increase in both GFP and BFP fluorescence levels (Fig. 4G), without a change in mRNA levels (Fig. S4H). In the case of ZNF598, however, knockdown led to the increase of GFP, but not BFP, indicating that the requirement for ZNF598 is specific to the Non-stop substrate, whereas alternative factors may be required to recruit GIGYF2 and 4EHP to No-Go mRNAs. Intriguingly, prior to the discovery of the RQC pathways, it had been suggested that the lack of a stop codon can interfere with translation of a message (Akimitsu et al., 2007). However, the relationship (if any) between that phenomenon, which was believed to act in a post-initiation step resulting in halting of translation before completion of full length proteins, and the GIGYF2/4EHP-mediated inhibition of translation of Non-stop and No-Go substrates is unclear.

Finally, to confirm that GIGYF2 and 4EHP are part of a pathway that works in parallel to RQC-mediated degradation of the stalled nascent polypeptide, we inhibited the proteasome by treating various knockdown cell lines with bortezomib (Fig. 4H). We observed stabilization of the stalled polypeptide in the *GIGYF2, 4EHP* and *ZNF598* knockdown cells lines of the same magnitude as cells expressing a control sgRNA, whereas, knockdown of *NEMF* leads to a much milder increase upon bortezomib treatment, consistent with the role of *NEMF* in UPS-mediated nascent chain degradation. This result indicates that the observed increase in fluorescence upon *GIGYF2* and *4EHP* knockdown is not caused by nascent chain stabilization, but by increased ribosome engagement, and that the partially synthesized polypeptide is still targeted for degradation by RQC.

The yeast homologs of GIGYF2, Smy2p and Syh1p, destabilize faulty mRNAs.

We next explored whether GIGYF2 and/or 4EHP played a role in RQC in yeast. Two potential homologs of GIGYF2 have been identified in yeast, Smy2p and Syh1p (Ash et al., 2010), although they have not been implicated in RQC. To determine if Smy2p and Syh1p

play a role in preventing accumulation of incomplete polypeptides, we utilized a previously characterized yeast stalling reporter (D'Orazio et al., 2019). This reporter expresses a no-go substrate and a control fluorescent protein from a bidirectional promoter. The stalling substrate encodes GFP separated by a T2A ribosome skipping sequence from *HIS3* gene containing an internal stretch of non-optimal codons (CGA_{12}). As a control, we used a similar reporter without the CGA12 stalling sequence. We compared the protein levels by flow cytometry and found that knockout of SMY2 and SYH1 alone led to an increase in the GFP/RFP ratio (Fig. 5A). Deleting both homologs led to a greater increase in GFP/RFP compared to the single deletions, suggesting that Smy2p and Syh1p have redundant function. This redundancy could account for the lack of identification of these factors in early RQC screens. Importantly, similar to the human homologs, deletion of the GYF-containing proteins had no effect on global translation (Fig. S4I). However, in contrast to the mammalian system, the increased expression of the reporter was accompanied by mRNA stabilization of the stalling mRNA, but not control mRNA (Fig. 5B, S4J). This observation is consistent with the apparent lack of a 4EHP homolog in yeast, which is an essential part of the mechanism of translation inhibition in mammals. Indeed, the yeast GIGYF2 homologs lack the 4EHP binding domain found in human GIGYF2 (Fig. 5C). However, Smy2p has been shown to bind Eap1p, a protein implicated in mRNA decapping and degradation (Ash et al., 2010). These data suggest that the role GIGYF2-like proteins play in RQC preceded the last common ancestor of yeast and mammals. Recruitment of GIGYF2 leads to translational silencing in higher eukaryotes, whereas Smy2p and Syh1p mediate RNA decay in yeast.

Recruitment of GIGYF2, 4EHP and ZNF598 leads to translation inhibition

Our genetic and biochemical data suggest that mammalian GIGYF2, 4EHP, and ZNF598 can inhibit translation on faulty mRNA (Fig. 4A), and that these three factors have buffering growth interactions with each other (Fig. 3D). These observations led to the hypothesis that the recruitment of GIGYF2 and 4EHP to problematic messages can be mediated at least in part by the ribosome collision detector, ZNF598 (Juszkiewicz and Hegde, 2017; Sundaramoorthy et al., 2017). To explore this hypothesis, we used an MS2-based system to tether ZNF598, GIGYF2, or 4EHP to a reporter mRNA (Bertrand et al., 1998) (Fig. 6A). We transiently co-expressed a non-stalling reporter ($GFP_{MS2\text{-}stop}$) harboring three MS2 stem-loops in its 5' UTR together with MS2 binding protein (MS2BP) fusions in HEK293T cells. Consistent with published data, recruitment of GIGYF2 or 4EHP to the reporter led to inhibition of translation (Kryszke et al., 2016), as evidenced by a robust decrease in GFP fluorescence without significant changes in the mRNA levels (Fig. 6B, Fig. S5A). The translation level was not strongly inhibited by MS2BP recruitment alone (Fig. 6B), or overexpression of a FLAG-tagged GIGYF2 protein that does not get recruited to the reporter (Fig. S5B, C), indicating that the observed translational silencing was specific for the tethering of the factors to the mRNA. Additionally, recruitment of ZNF598 to the reporter induced similar translational silencing.

To explore the genetic requirements for translation inhibition, we generated stable cell lines expressing an MS2-fusion protein, as well as $GFP_{MS2\text{-}stop}$ reporter, and CRISPRi machinery (Fig. 6C, S5D). We used CRISPRi to knock down *ZNF598*, *GIGYF2*, or *4EHP* and

measured the effect of the knockdown on GFP levels via flow cytometry. Knockdown of *GIGYF2* or *4EHP* alleviated the decrease in GFP fluorescence caused by MS2-ZNF598 (Fig. 6D). Lower expression of the MS2BP-GIGYF2 fusion protein in K562 cells resulted in an attenuated repression phenotype compared to HEK293T (Fig. S5E). Nonetheless, the GIGYF2-mediated repression depended on 4EHP. Similarly, 4EHP-mediated repression depended on GIGYF2, suggesting that these two factors act together to mediate translation inhibition (Fig. 6D, S6A–H). In marked contrast, silencing by neither GIGYF2, nor by 4EHP was impacted by knockdown of *ZNF598* when these factors were directly recruited to the mRNA, indicating that GIGYF2 and 4EHP work downstream and independently of ZNF598. These epistasis experiments support a model in which ZNF598 serves as a scaffold that can recruit GIGYF2 and 4EHP to faulty mRNAs (Fig. 6E) and argue against a model in which ZNF598-mediated translational repression of damaged mRNA represents a distinct, GIGYF/4EHP independent pathway.

Translational inhibition by ZNF598 is mediated by GIGYF2 and 4EHP in a ubiquitination-independent manner.

ZNF598 recognizes collided stalled ribosomes and ubiquitinates the small subunit of the ribosome, which triggers ribosome splitting and subsequent RQC complex engagement (Ikeuchi et al., 2019; Juszkiewicz et al., 2018). We next tested whether ZNF598-mediated ubiquitination is required for translational repression by GIGYF2 and 4EHP. We generated ubiquitination-deficient MS2BP-ZNF598 fusion proteins that harbored inactivating mutations in the RING domain (C29A) or deletions of the entire domain (ΔRING) (Sundaramoorthy et al., 2017) and compared their ability to translationally silence the $GFP_{MS2\text{-}stop}$ reporter. Surprisingly, both mutants were capable of repressing translation (Fig. 6F, S6I). Recruitment of a stably integrated MS2BP-ZNF598ΔRING also repressed translation in a GIGYF2 and 4EHP-dependent manner matching the recruitment of wild-type ZNF598. (Fig. 6G, S6J). These data suggest that ZNF598 has a dual function when it engages collided ribosomes. It serves as a ubiquitin ligase that mono-ubiquitinates the 40S small subunit, triggering release of the stalled ribosome and subsequent RQC engagement, and nascent polypeptide degradation (Juszkiewicz et al., 2018; Sundaramoorthy et al., 2017). In addition, ZNF598 also serves as a scaffold that provides one mechanism for the recruitment of GIGYF2 and 4EHP to the mRNA, in a ubiquitination-independent manner. Once recruited, GIGYF2 and 4EHP sequester the mRNA cap, blocking ribosome initiation and decreasing the translational load on problematic messages (Fig. 7D).

GIGYF2 and 4EHP can be recruited to faulty mRNAs in a ZNF598-independent manner.

The translation phenotype of *ZNF598* knockdown is consistently weaker than that seen with *GIGYF2* knockdown alone for Non-stop substrates (Fig. 3A, 7A) and ZNF598, unlike GIGYF2, does not have a translational effect on our No-go reporter (Fig. 4E). Moreover, when *GIGYF2* is knocked down, additional depletion of *ZNF598* has no effect on the increased translation of the $GFP_{Non\text{-}stop}$ reporter (Fig. 7A, S7A). This phenomenon is recapitulated by the artificial tethering experiments using MS2; ZNF598 relies on GIGYF2 or 4EHP for translation repression, but GIGYF2 and 4EHP do not require ZNF598 for translational repression when directly recruited to the message. These observations can be explained by the presence of alternative recruitment mechanisms for GIGYF2 and 4EHP to

faulty mRNAs, or by technical limitations, such as incomplete *ZNF598* knockdown. Although we achieved over 95% knockdown of *ZNF598* via CRISPRi (Fig. 7B, S7B), we could not exclude the possibility that the remaining ZNF598 is responsible for the observed partial phenotype. To differentiate between these two hypotheses, we engineered a *ZNF598* knockout cell line using CRISPR/Cas9 and confirmed that these cells are true knockouts both by western blotting (Fig. 7B, S7B) and sequencing of the genomic locus (Canaj et al., 2019). We integrated the $GFP_{Non\text{-}stop}$ reporter in these cells and measured the effect of *GIGYF2* and *4EHP* knockdown on the GFP and BFP levels. Knocking down these factors led to an increase in both the GFP and BFP fluorescent signals, even though no ZNF598 is present in these cells (Fig. 7C). Importantly, knockdown of *ZNF598* in the knockout cells had no effect on the stalling reporter, confirming the specificity of the CRISPRi knockdown. This experiment supports the existence of ZNF598-independent recruitment mechanism(s) that enable GIGYF2 and 4EHP to inhibit translation of damaged messages (Fig. 7D)

Discussion:

The cell faces an inherent challenge in detecting problematic mRNAs in that it is only through the act of translation itself that the lesion can be recognized, and failure of this recognition results in cytotoxicity. Our work reveals a novel mechanism in which failed translation leads to inhibition of further translation initiation on that message. This pathway acts in parallel with previously described quality control pathways, which trigger mRNA degradation, ribosome release, and proteasomal degradation of the stalled nascent polypeptide. Without a mechanism to block further initiation on problematic messages, translation of faulty mRNAs would continue for as long as the message persists. GIGYF2 and 4EHP enable the cell to break this cycle by allowing a failed translation event to initiate a specific negative feedback loop which shuts down further translation of the message. Although GIGYF2 and 4EHP have been implicated in translational control in a number of different settings (Amaya Ramirez et al., 2018; Fu et al., 2016; Kryszke et al., 2016; Morita et al., 2012; Peter et al., 2017; Tollenaere et al., 2019), our data argue that faulty mRNAs that cause ribosome stalling comprise an important subset of endogenous substrates for GIGYF2 and 4EHP mediated repression. Indeed, loss of GIGYF2 specifically increases translational output from two distinct classes of stalling reporters. Moreover, knocking down GIGYF2 in combination with loss of RQC components had a strong synergistic growth interaction in the absence of a reporter, suggesting that there is a continuous production of endogenous stalling substrates that engage RQC.

How then are stalled ribosomes recognized and how is GIGYF2 recruited? Recruitment of GIGYF2 and 4EHP to their endogenous substrate is hypothesized to occur via sets of auxiliary RNA binding proteins that serve as adapters. Our data argue that ZNF598 can serve as one such adapter to recruit the inhibitory complex to defective messages. However, GIGYF2 and 4EHP are still capable of repressing translation initiation on faulty mRNAs even in a ZNF598 null background (Fig. 7B, C). These data suggest that there are both ZNF598-dependent and ZNF598-independent mechanisms for recruitment of GIGYF2 and 4EHP to mediate translation inhibition on defective messages (Fig. 7D). The identity of these additional adapters and whether they are redundant with ZNF598, activated or

expressed as a compensatory mechanism upon ZNF598 loss, or act on specific classes of faulty mRNAs remains to be explored.

How is translation initiation inhibited? Since 4EHP is a cap binding protein, one might naively expect that GIGYF2 and 4EHP will exclusively affect cap-dependent translation. However, further considerations suggest that GIGYF2 and 4EHP may have a broader effect on translation. For example, GIGYF2 contains a Glycine/Tryptophan (GW)-rich motif that has been shown to facilitate phase transition (Sheu-Gruttadauria and MacRae, 2018). Thus, an attractive hypothesis is that upon stalling, messages bound by GIGYF2 are sequestered away in an inhibitory environment that further interferes with translation, in addition to the direct inhibitory effect of 4EHP-mediated cap sequestration. In support of this hypothesis, using single mRNA imaging in live cells Moon and colleagues (Moon et al., 2020) observed that messages that contain stalled ribosomes can partition into stress granules under different cellular conditions. As a result, the molecular mechanism by which GIGYF2 and 4EHP mediate translational repression upon ribosome stalling is likely multidimensional and remains to be fully explored.

Regardless of their recruitment or silencing mechanism, our data establish a critical role for GIGYF2 and 4EHP in inhibiting translation initiation on defective mRNAs. The synergistic growth defects with core RQC components highlight the importance of these two factors in preventing accumulation of incomplete proteins. Loss of GIGYF2 has been associated with neurodegenerative and neurodevelopmental phenotypes (Krumm et al., 2015; Thyme et al., 2019), similar to loss of RQC components (Chu et al., 2009). It is tempting to speculate that dysregulation of the GIGYF2/4EHP pathway increases the burden on the proteostasis network in neurons. As these cells age, they can either accumulate defective mRNAs or become less efficient in detecting and/or coping with stalled ribosomes. If these cells lack functional GIGYF2 and 4EHP to translationally silence such defective messages, the increased stalling burden may overwhelm the RQC pathway in cells leading to cell stress and neurodegenerative disease.

RESOURCE AVAILABILITY

Lead Contact

Further information and requests for resources and reagents should be directed to and will be fulfilled by the Lead Contact, Jonathan S. Weissman (jonathan.weissman@ucsf.edu).

Materials Availability

All plasmids and cell lines generated in this study are available upon request and will be fulfilled by the lead contact, Jonathan S. Weissman (jonathan.weissman@ucsf.edu).

Data and Code Availability

CRISPRi genome-scale screen gene-level phenotype is available in Tables S4–5. Ribosome profiling and RNAseq sequencing files have been uploaded to Gene Expression Omnibus (GEO) with identifier GSE153597. Mass Spectrometry data is available in Table S6, and has been uploaded to PRIDE database, data are available via ProteomeXchange with identifier

PX019961. Full western blot images used in this study can be found on Mendeley Data: http://dx.doi.org/10.17632/j42j59f9hf.1

EXPERIMENTAL MODEL AND SUBJECT DETAILS

K562 cells were grown in RPMI-1640 with 25mM HEPES, 2.0 g/L NaHCO3, 0.3 g/L L-Glutamine supplemented with 10% FBS, 2 mM glutamine, 100 units/mL penicillin and 100 μg/mL streptomycin. HEK293T cells were grown in Dulbecco's modified eagle medium (DMEM) in 10% FBS, 2 mM glutamine, 100 units/mL penicillin and 100 μg/mL streptomycin. K562 cells are derived from female patients/donors. HEK293T are derived from a female fetus. All cell lines were grown at 37 degrees Celsius.

METHOD DETAILS

Generation of reporter cell lines

Reporter constructs ($GFP_{Non\text{-}stop}$, GFP_{Stop}, GFP_{PolyA}, K20, $RFP_{Non\text{-}stop}$, RFP_{Stop}, $GFP_{MS2\text{-}stop}$, MS2BP, MS2BP-ZNF598, MS2BP-GIGYF2, MS2BP-4EHP) were stably transduced into K562 CRISPRi cell line (Horlbeck et al., 2016) using Piggy-Bac transposition (System Biosciences PB210PA-1 and corresponding Piggy-Bac expression vector Table S1). Positive cells were isolated by FACS on a BD FACSAria2.

Transient expression of reporters ($GFP_{Non\text{-}stop}$, GFP_{Stop}, GFP_{PolyA}, MS2BP, MS2BP-ZNF598, MS2BP-GIGYF2, MS2BP-4EHP) was achieved by transfecting HEK293T cells with vectors from Table S1 using TransIT-LTI Transfection Reagent (Mirus, MIR 2306) according to the manufacturer's instructions.

Generation of GFP11-GIGYF2 cell line

GFP11-GIGYF2 tagged HEK293T cells were generated as previously described (Leonetti *et al.*, PNAS, 2016), using targeting sgRNA (AATACGGAACAGAATGGCAG) and ssDNA oligo(TATTTTTCTCGTTAACAGGTTTCTTCACATATAAAAATCTATTGTAAAAATACGGAAAAGAatgcgtgaccacatggtccttcatgagtatgtaaatgctgctgggattacaGGCGGTGGAGGGAGTggcggaggtGGATCCGCAGCGGAAACGCAGACACTGAACTTTGGGCCTGAATGGTGAGTTTTCAAAATCTCAT).

Generation of ZNF598 knockout cell line

ZNF598 knockout cell line was generated by transfecting K562 CRISPRi cells with an all-in-one vector pSpCas9(BB)-2A-GFP (PX458) (Addgene plasmid #48138). This vector was modified to express two sgRNAs targeting ZNF598 [ACCGCTGCTCTACCAAGATG], [ATGGGGACTTTGCCTCACTG]. Three days post transfection, GFP positive cells were sorted into single cells. These clones were expanded and ZNF598 knockout was confirmed by western blot for protein expression (Bethyl Laboratories, A305–108A-T), and genotyped with Genewiz amplicon-ez sequencing. The CRISPR-Cas9 induced genome edits were identified by using the computational pipeline developed by (Canaj et al., 2019).

Genome-scale CRISPRi screening

Genome-scale screens were conducted similar to previously described screens ((Gilbert et al., 2014; Horlbeck et al., 2016). The CRISPRi compact library (5 sgRNA/TSS) CRISPRi-v2 (Addgene, Cat#83969) were transduced in duplicate into K562 CRISPRi cells at MOI < 1 (percentage of transduced cells 2 days after transduction: 20%–40%). Replicates were maintained separately in 1.5 L of RPMI-1640 in 3 L spinner flasks for the course of the screen. 2 days after transduction, the cells were selected with 1 mg/mL puromycin for 2 days, until transduced cells accounted for 80%–95% of the population. The cells were maintained in spinner flasks by daily dilution to $0.5 \cdot 10^6$ cells /mL at an average coverage of greater than 500 cells per sgRNA for the duration of the screen. Genomic DNA was isolated from frozen cells, and the sgRNA-encoded regions were enriched, amplified, and prepared for sequencing as described previously (Gilbert et al., 2014).

FACS-based CRISPRi screen

Cells were sorted using BD FACS Aria2 2 days after recovery from puromycin selection based on GFP fluorescence of $GFP_{Non\text{-}stop}$ reporter. Cells with the highest (~30%) and lowest (~30%) GFP expression were collected and immediately frozen. Approximately 30 million cells were collected per group.

Growth-based CRISPRi Screen

K562 CRISPRi cells were infected with control sgRNA or sgRNA targeting *NEMF* which also expressed RFP. RFP positive cells were sorted on a BD FACSAria2. Both cell lines were infected with the hCRISPR-v2 library. 100,000 cells from both cell lines were harvested after recovery from puromycin selection as Day 0, and then again after 10 doublings.

Processing of CRISPRi screen data

Sequencing reads were aligned to the CRISPRi v2 library sequences, counted, and quantified using the Python-based ScreenProcessing pipeline (https://github.com/mhorlbeck/ScreenProcessing; (Horlbeck et al., 2016). Generation of negative control genes and calculation of phenotypes and Mann-Whitney p-values was performed as described previously (Gilbert et al., 2014; Horlbeck et al., 2016). GFP phenotypes were calculated from the top 30% GFP sorted samples, divided by the bottom 30% GFP. Phenotypes from sgRNAs targeting the same gene were collapsed into a single GFP stabilization phenotype using the average of the top three scoring sgRNAs (by absolute value) and assigned a p-value using the Mann-Whitney test of all sgRNAs targeting the same gene compared to the non-targeting controls. All additional CRISPRi screen data analyses were performed in Python 2.7 using a combination of Numpy (v1.12.1), Pandas (v0.17.1), and Scipy (v0.17.0). For all experiments, details of quantification and statistical methods used are described in the corresponding figure legends or results sections. Gene-level phenotypes and counts are available in Tables S4–5.

Individual evaluation of sgRNA phenotypes

Single sgRNA expression vectors were individually cloned by annealing complementary synthetic oligonucleotide pairs (Integrated DNA Technologies) for each sgRNA with flanking BstXI and BlpI restriction sites and ligating the resulting double-stranded segment into either BstXI/BlpI-digested pCRISPRi-v2 (marked with a puromycin resistance cassette and BFP similar to (Horlbeck et al., 2016) or BstXI/BlpI-digested pU6-sgRNA EF1a-puro-t2a-mCherry (marked with a puromycin resistance cassette and RFP).

Dual sgRNA expression vectors were assembled by a two-step cloning procedure. First, sgRNAs to be included were cloned into the corresponding individual sgRNA expression vectors. sgRNAs destined for the first position of the dual sgRNA vector were cloned into either pMJ002 or pCRISPRia-v2 (Addgene #84832), which both contain a mU6 promoter for sgRNA expression, and sgRNAs destined for the second position were cloned into pMJ003, which contains a hU6 promoter for sgRNA expression. All vectors contain the same constant region and pMJ002 and pMJ003 contain specific primer binding sites flanking the sgRNA expression cassette. Complementary oligonucleotides (Integrated DNA Technologies) containing the sgRNA sequence and ligation overhangs were annealed and ligated into the corresponding BstXI/BlpI-digested sgRNA expression vectors. Single clones from this procedure were used as templates for the second assembly step, in which the sgRNA expression cassettes containing the U6 promoter, sgRNA sequence, and constant region were assembled into a vector backbone containing a puromycin resistance marker and BFP (pCRISPRia-v2 [Addgene #84832]) or mCherry (a version of pU6-sgCXCR4–2 [Addgene #46917] modified to include a BlpI site). The desired sgRNA expression cassettes were PCR-amplified (pMJ002-based constructs: oMJ0767 [GTTAGTACCGGGCCCGC] and oMJ0768 [CCATAGCTGAGTGTAGATTCGAGCAAAAAAAGCACCGACTCGG]; pCRISPRia-v2-based constructs: oMJ0873 [CCAGTTTGGTTAGTACCGGGCCCGCTCTAGAGATCCGACGCGC] and oMJ0768; pMJ003-based constructs: oMJ0612 [GCTCGAATCTACACTCAGCTATGG] and oMJ0613 [GCCGCCTAATGGATCCTAG]) and inserted into XbaI/XhoI-digested backbone by a single three-piece Gibson assembly step.

Protospacer sequences used for individual evaluation are listed in Table S2. The resulting sgRNA expression vectors were individually packaged into lentivirus. These sgRNA vectors were transduced into K562-dCas9 cells expressing $GFP_{Non\text{-}stop}$ at MOI < 1 (20 – 40% infected cells). BFP and GFP protein levels were measured by flow cytometry at day 5 post infection. Median fluorescent values were calculated for each cell line using FlowJo software and compared fluorescent levels after sgRNA knockdown to a cell line expressing to a non-targeting sgRNA. All additional data analyses were performed in Python 2.7 using a combination of Numpy, Pandas, Scipy, and Cytoflow.

Internally controlled growth assays

Dual sgRNA growth phenotypes were performed by transducing cells with dual sgRNA expression constructs at MOI < 1 (15 – 30% infected cells). The fraction of sgRNA-expressing cells was measured from 4–16 days after infection by flow cytometry on an LSR-II (BD Biosciences). A population of infected cells was selected to purity with puromycin (1

mg/mL), allowed to recover for 2 days, and harvested for measurement of mRNA levels by RT-qPCR (see below). Experiments were performed in duplicate from the infection step. The expected double phenotype score was calculated by adding the phenotype of both sgRNAs on day 16. Epistasis was measured by subtracting the expected phenotype from the measured phenotype of dual knockdowns.

Yeast fluorescent assay and qPCR

All strains used in this study are listed in the key resources table. Strain BY4741 was used as the wild-type parental strain. Genomic knockouts were generated by one-step gene replacement as previously described (Rothstein, 1991). Flow cytometry measurements were performed as previously described (D'Orazio et al., 2019). RNA was isolated from yeast cells in mid log phase as previously described (Ares, 2012). Residual DNA was removed with DNA-freeTM DNA Removal Kit (Thermo Fisher Scientific). RNA was converted to cDNA using AMV Reverse Transcriptase (Promega) under standard conditions with Random Primer Mix (NEB, S1330S). Quantitative PCR reactions were prepared with SsoAdvanced™ Universal SYBR Green Supermix (Bio-RAD, 1725270) according to the manufacturer's instructions. Reactions were run on a Bio-RAD CFX96 Touch Real-Time PCR Detection System. Primer sequences are listed in supplemental table S3.

Ribosome Profiling

K562 CRISPRi cells stably expressing $GFP_{Non\text{-}stop}$ was infected with lentiviral vectors containing a guide RNA against one gene or non-targeting guide RNA (Table S2). Cells were selected using FACS to recover cells containing sgRNA (labeled with RFP). Cyclohexamide was added (100mg/ul) to the cells and they were incubated for 5 minutes at 37 °C and then pelleted at 400g for 5 minutes. Media was removed and cell pellets were immediately snap frozen. Libraries were prepared according to (McGlincy and Ingolia, 2017).

Ribosome profiling and RNAseq analysis

Ribosome profiling and RNA-seq libraries were sequenced on an Illumina HiSeq 4000 as single end 50-bp reads (UCSF Center for Advanced Technology) at a depth of 22–64 million reads per library. Ribosome profiling reads were processed by removing 3' linker sequences using *FASTX clipper* and de-multiplexed using *FASTX barcode splitter* (http://hannonlab.cshl.edu/fastx_toolkit/). Sample barcodes and unique molecular identifiers were trimmed using a custom Python script. Next, abundant reads were filtered by aligning to a custom library of human rRNAs, tRNAs, and primer sequences using *bowtie* v1.2 (http://bowtie-bio.sourceforge.net/). All remaining reads were aligned to a modified human genome (GRCh38.92 with addition of our CRISPRi construct and the $GFP_{Non\text{-}stop}$) using *tophat* v2.1.1 (https://ccb.jhu.edu/software/tophat/; relevant parameters: --read-mismatches=1 and --no-novel-juncs). After alignment, uniquely mapping reads were extracted, and *plastid* (https://plastid.readthedocs.io) was used to obtain gene-level read counts and normalized counts, reads per kilobase per million mapped reads (RPKM). To assign reads to genomic positions, a p-site offset of 12 nucleotides was determined by calculating the average distance of the start codon peak from the start codon (*plastid psite*). To assess the quality of the ribosome profiling data, we confirmed that the aligned reads displayed the expected

three nucleotide periodicity (phasing) and that the majority of ribosome footprints had a length of 28–31 bp for all libraries. We also confirmed that the CRISPRi system produced robust target knockdown on the day of the experiment at the level of ribosome footprints (knockdown of target genes >88% for all genes). The RNA-seq libraries were processed using the same pipeline as the ribosome profiling libraries, with the exception that *tophat* was run with –read-mismatches=2 due to the longer RNAseq read length. All downstream analyses were performed using the Python libraries pandas, plastid, matplotlib, seaborn, numpy, and scipy.

For Figure S1A, footprints from K562 CRISPRi cells bearing non-targeting sgRNA are plotted as reads per million. Here, we plotted all aligned reads rather than uniquely aligned reads to visualize read density in the $GFP_{Non\text{-}stop}$ MALAT1 triple helix, which is identical to the endogenous MALAT1 lncRNA. To confirm that the reads aligning to the MALAT1 triple helix in the $GFP_{Non\text{-}stop}$ are not derived from the endogenous MALAT1 lncRNA, we performed ribosome profiling in a K562 CRISPRi cell line without the $GFP_{Non\text{-}stop}$ reporter. Here, we found that the endogenous MALAT1 background rate was <10% of the $GFP_{Non\text{-}stop}$ footprints in the MALAT1 triple helix, suggesting that the $GFP_{Non\text{-}stop}$ triple helix is indeed translated. For Figure S5A, translational efficiencies were calculated by normalizing the $GFP_{Non\text{-}stop}$ GFP ribosome footprint rpm to the $GFP_{Non\text{-}stop}$ RNAseq rpm.

RNA sequencing

RNA was extracted using Zymo mini RNA prep (R2053) and libraries were cloned using Illumnia true stranded total RNA seq kit (20020596).

RT-qPCR

Total RNA was isolated from frozen cell samples using TRIzol reagent (Thermo Fisher Scientific) and Phase Lock Gel tubes (VWR), treated with Turbo DNase (Thermo Fisher Scientific), or using Direct-zol RNA MiniPrep kit. Reverse-transcription was carried using M-MLV (Thermo Fisher Scientific) or SSIII Reverse-transcriptase (Thermo Fisher Scientific) with random hexamer primers (Thermo Fisher Scientific, SO124) in the presence of RNaseIN Recombinant Ribonuclease Inhibitor (Thermo Fisher Scientific). Quantitative PCR (qPCR) was performed with Kappa Sybr Fast qPCR 2x Mix (Roche), according to the manufacturer's instructions on a LightCycler 480 Instrument (Roche). Experiments were performed in technical triplicates. RT-qPCR primers used are listed in (Table S3).

Immunoprecipitation and western blot

Cells were lysed in buffer containing 10mM Tris 7.5, 150 mM NaCl, 0.5% NP-40, 5 mM Mg_2Cl, and 1x Halt™ Protease Inhibitor Cocktail (Thermo Fisher Scientific). The lysates were cleared by centrifugation at 20,000 × g for 10 min and bound to GFP-Trap Magnetic Beads (Chrometech) for 2h at 4 °C. Beads were washed 3 times with IP Buffer (10mM Tris 7.5, 150 mM NaCl, 0.1% NP-40, 5 mM Mg_2Cl). Bound material was eluted by boiling in Laemmli Buffer for 10 min at 90°C.

Proteins were separated on Bolt® 4–12% Bis-tris gels (Thermo Fisher Scientific), transferred to PVDF membrane using the Mini Trans-Blot Cell (Bio-Rad) according to the

manufacturer's instructions, blocked with 5% milk in TBS, and subsequently probed. Rabbit anti ZNF598 antibody (Bethyl Laboratories, A305–108A-T), rabbit anti GIGYF2 antibody (Bethyl Laboratories, A303–731A-M), and rabbit anti 4EHP antibody (Cell Signaling, 6916S) primary antibodies were used. LI-COR IRDye800/IRDye700 anti-rabbit (Odyssey) secondary antibody was used at 1:10,000 dilution. All blots were visualized using the LI-COR (Odyssey) system.

ZNF598 Mass Spectrometry cell line generation

3X-FLAG-tagged ZNF598 overexpressing (ZNF598-OE) Flp-In T-Rex 293 cells (kind gift from Dr. Nahum Sonenberg and Dr. Thomas Tuschl, (Garzia et al., 2017) were grown in high-glucose Dulbecco's Modified Eagle Medium (Thermo Fisher, 11995040, containing 4 mM L-Glutamine and 1 mM sodium pyruvate) supplemented with 10% (v/v) fetal bovine serum. The affinity purification mass spectrometry experiment was performed in biological triplicate. Two million low-passage cells were seeded per 10 cm dish. Expression of 3X-FLAG-tagged ZNF598 was induced (24 hours post seeding) for 24 hours by the addition of doxycycline at 1 μg/ml at final concentration.

FLAG-immunoprecipitation of 3X-FLAG-ZNF598 from HEK293 cells

Cells were washed with warm PBS (containing 360 μM emetine), and harvested in ice-cold lysis buffer (50 mM TRIS pH 8.0, 150 mM KCl, 15 mM $MgCl_2.6H_2O$, 5% glycerol) supplemented with 1% Triton X-100, 360 μM emetine, 20 mM N-ethylmaleimide, 80 units TURBO DNase (Thermo Fisher, AM2238) and protease inhibitors (cOmplete Protease Inhibitor Cocktail, Roche; Protease Inhibitor Cocktail, Millipore Sigma; and PMSF, Millipore Sigma). Cell lysates were clarified in a tabletop micro-centrifuge (15 minutes, 4°C). Equal protein amounts from the clarified supernatant were used for each immunoprecipitation. The clarified supernatant was incubated with ANTI-FLAG-Agarose M2 affinity gel (Millipore Sigma #A2220, 15 μl of packed affinity resin) for 1 hour, washed four times with 400 μl wash 1 buffer (lysis buffer supplemented with 0.1% Triton X-100 and 360 μM emetine), then washed four times with wash 2 buffer (50 mM TRIS pH 8.0, 150 mM KCl, 15 mM $MgCl_2.6H_2O$ supplemented with 360 μM emetine), and eluted in 80 μl elution buffer (50 mM TRIS pH 8.0, 150 mM KCl, 15 mM $MgCl_2.6H_2O$ supplemented with 400 μg/ml 3X FLAG-peptide (Millipore Sigma, #F4799)). Eluates were flash frozen in liquid nitrogen and stored at -80°C prior to protein digestion.

Protein Digestion

Protein extracts (4 μg) were diluted up to 300 μl in 10 mM triethyl ammonium bicarbonate (TEAB) and were reduced with 15 μl of 7.5 mg/ml DL-dithiothreitol (DTT) (60°C, 1 hour). After cooling to room temperature, samples were alkylated with 15 μl of 18.5 mg/ml iodoacetamide for 15 minutes at room temperature in the dark. Reduced and alkylated proteins were buffer-exchanged on a 30 kDa molecular weight spin cartridge (Amicon Ultra 0.5 ml, Millipore Sigma) and washed four times with 400 μl 10 mM TEAB. Proteins were digested overnight at 37°C on the filter with 300 μl Trypsin (20 μg in 3 ml 10 mM TEAB, Promega Sequencing Grade Modified Trypsin). Additional Trypsin (100 μl of 10 mg/ml) was added the next morning (37°C, 1 hour). Peptides were removed from the top of the filter

and the filter was washed twice with 300 2% acetonitrile, 0.1% formic acid. All washes were combined and dried.

Liquid Chromatography and Mass Spectrometry

Liquid Chromatography and Mass Spectrometry was performed at the Mass Spectrometry and Proteomics Core, JHMI. Peptides were analyzed by liquid chromatography interfaced with tandem mass spectrometry (LC/MS/MS) using a Waters nanoACQUITY UPLC system (www.waters.com) interfaced with an Orbitrap Fusion™ Lumos™ Tribrid™ Mass Spectrometer (www.thermofisher.com). Fractions were resuspended in 20 µl loading buffer (2% acetonitrile in 0.1% formic acid) and analyzed by reverse phase liquid chromatography coupled to tandem mass spectrometry. Peptides (50%, approx. 1 µg) were loaded onto a C18 trap (S-10 µM, 120 Å, 75 µm × 2 cm, YMC, Japan) and subsequently separated on an in-house packed PicoFrit column (75 µm × 200 mm, 15u, +/-1 µm tip, New Objective) with C18 phase (ReproSil-Pur C18-AQ, 3 µm, 120 Å, www.dr-maisch.com) using 2–90% acetonitrile gradient at 300 nl/min over 120 min. Eluting peptides were sprayed at 2.0 kV directly into the Lumos.

Survey scans (full MS) were acquired from 350–1800 m/z with data-dependent monitoring with a 3 sec cycle time. Each precursor individually isolated in a 1.6 Da window and fragmented using HCD activation collision energy 30 and 15 sec dynamic exclusion, first mass being 120 m/z. Precursor and fragment ions were analyzed at resolutions 120,000 and 30,000, respectively, with automatic gain control (AGC) target values at 4e5 with 50 ms maximum injection time (IT) and 1e5 with 100 ms maximum IT, respectively.

Processing of Mass Spectrometry Data

Raw data was processed and analyzed using the MaxQuant software suite (Cox and Mann, Nature Biotechnology, 2008). Default settings were used except that ‘Match between runs’ was turned on to transfer peptide identification from an LC-MS run, in which the peptide has been identified by MS/MS, to another LC-MS run, in which no MS/MS data for the same peptide was acquired or no peptide was assigned (Tyanova et al., 2016). Search parameters were as follows: a maximum of two missed cleavages were allowed, cysteine carbamidomethyl was included as a fixed modification, and variable modifications included oxidation of methionine, protein N-terminal acetylation, deamidation of glutamine and asparagine, phosphorylation of serine, threonine and tyrosine, and Gly-Gly ubiquitin remnant on lysine. Database search was performed with Andromeda (Cox and Mann, 2008; Cox et al., 2011) against Uniprot human database (UP000005640_9606.fasta; downloaded on 09/10/2018) with common serum contaminants and enzyme sequences. False discovery rate (FDR) was set to 1% at both the peptide spectrum match (PSM) and protein level. A minimum peptide count required for protein quantification was set to two. Protein groups were further analyzed using the Perseus software suite. Common contaminants, reverse proteins and proteins only identified by site were filtered out. LFQ values were transformed to $\log_2$ space and intensity distributions were checked to ensure that data was normally distributed.

QUANTIFICATION AND STATISTICAL ANALYSIS

For all experiments, details of quantification and statistical methods are described in the corresponding figure legends and methods section.

Supplementary Material

Refer to Web version on PubMed Central for supplementary material.

Acknowledgements:

We thank M. Shurtleff and A. Mizrak for scientific input and helpful discussions, R. Pak and P. Solomon for help with genetic screens, K. Popova for advice on knockout cell line generation, and G. Ow and E. Collisson for sharing the mCherry-marked sgRNA expression vector. This work was supported by NIH Center for RNA Systems Biology (J.S.W.), NIH Directors' Early Independence Award 1DP5OD028147-01 (K.K.), UCSF Genentech Fellowship (K.L.H.), HHMI Faculty Scholar award (A.F.), and NIH grants NIH 5R01AG041826-05 (J.S.W.) and K99 GM130964 (M.J.). J.A.H. is the Rebecca Ridley Kry Fellow of the Damon Runyon Cancer Research Foundation (DRG-2262-16). A.F. is a Chan Zuckerberg Biohub investigator. J.S.W and R.G. are Howard Hughes Medical Institute Investigators.

References:

Akimitsu N, Tanaka J, and Pelletier J (2007). Translation of nonSTOP mRNA is repressed post-initiation in mammalian cells. EMBO J. 26, 2327–2338. [PubMed: 17446866]

Amaya Ramirez CC, Hubbe P, Mandel N, and Béthune J (2018). 4EHP-independent repression of endogenous mRNAs by the RNA-binding protein GIGYF2. Nucleic Acids Res. 46, 5792–5808. [PubMed: 29554310]

Ares M (2012). Isolation of total RNA from yeast cell cultures. Cold Spring Harb. Protoc 7, 1082–1086.

Ash MR, Faelber K, Kosslick D, Albert GI, Roske Y, Kofler M, Schuemann M, Krause E, and Freund C (2010). Conserved β-hairpin recognition by the GYF domains of Smy2 and GIGYF2 in mRNA surveillance and vesicular transport complexes. Structure 18, 944–954. [PubMed: 20696395]

Bengtson MH, and Joazeiro CAP (2010). Role of a ribosome-associated E3 ubiquitin ligase in protein quality control. Nature 467, 470–473. [PubMed: 20835226]

Bertrand E, Chartrand P, Schaefer M, Shenoy SM, Singer RH, and Long RM (1998). Localization of ASH1 mRNA Particles in Living Yeast. Mol. Cell 2, 437–445. [PubMed: 9809065]

Brandman O, Stewart-Ornstein J, Wong D, Larson A, Williams CC, Li G-W, Zhou S, King D, Shen PS, Weibezahn J, et al. (2012). A ribosome-bound quality control complex triggers degradation of nascent peptides and signals translation stress. Cell 151, 1042–1054. [PubMed: 23178123]

Canaj H, Hussmann JA, Li H, Beckman KA, Goodrich L, Cho NH, Li YJ, Santos DA, McGeever A, Stewart EM, et al. (2019). Deep profiling reveals substantial heterogeneity of integration outcomes in CRISPR knock-in experiments. BioRxiv 841098.

Choe Y-J, Park S-H, Hassemer T, Körner R, Vincenz-Donnelly L, Hayer-Hartl M, and Hartl FU (2016). Failure of RQC machinery causes protein aggregation and proteotoxic stress. Nature 531, 191–195. [PubMed: 26934223]

Chu J, Hong NA, Masuda CA, Jenkins BV, Nelms KA, Goodnow CC, Glynne RJ, Wu H, Masliah E, Joazeiro CAP, et al. (2009). A mouse forward genetics screen identifies LISTERIN as an E3 ubiquitin ligase involved in neurodegeneration. Proc. Natl. Acad. Sci 106, 2097–2103. [PubMed: 19196968]

Cox J, and Mann M (2008). MaxQuant enables high peptide identification rates, individualized p.p.b.-range mass accuracies and proteome-wide protein quantification. Nat. Biotechnol 26, 1367–1372. [PubMed: 19029910]

Cox J, Neuhauser N, Michalski A, Scheltema RA, Olsen JV, and Mann M (2011). Andromeda: A peptide search engine integrated into the MaxQuant environment. J. Proteome Res 10, 1794–1805. [PubMed: 21254760]

D'Orazio KN, Wu CC-C, Sinha N, Loll-Krippleber R, Brown GW, and Green R (2019). The endonuclease Cue2 cleaves mRNAs at stalled ribosomes during No Go Decay. Elife 8.

Defenouillère Q, Yao Y, Mouaikel J, Namane A, Galopier A, Decourty L, Doyen A, Malabat C, Saveanu C, Jacquier A, et al. (2013). Cdc48-associated complex bound to 60S particles is required for the clearance of aberrant translation products. Proc. Natl. Acad. Sci. U. S. A 110, 5046–5051. [PubMed: 23479637]

Doma MK, and Parker R (2006). Endonucleolytic cleavage of eukaryotic mRNAs with stalls in translation elongation. Nature 440, 561–564. [PubMed: 16554824]

Frischmeyer PA, Van Hoof A, O'Donnell K, Guerrerio AL, Parker R, and Dietz HC (2002). An mRNA surveillance mechanism that eliminates transcripts lacking termination codons. Science (80-.).

Fu R, Olsen MT, Webb K, Bennett EJ, and Lykke-Andersen J (2016). Recruitment of the 4EHP-GYF2 cap-binding complex to tetraproline motifs of tristetraprolin promotes repression and degradation of mRNAs with AU-rich elements. RNA 22, 373–382. [PubMed: 26763119]

Garzia A, Jafarnejad SM, Meyer C, Chapat C, Gogakos T, Morozov P, Amiri M, Shapiro M, Molina H, Tuschl T, et al. (2017). The E3 ubiquitin ligase and RNA-binding protein ZNF598 orchestrates ribosome quality control of premature polyadenylated mRNAs. Nat. Commun 8.

Gilbert LA, Horlbeck MA, Adamson B, Villalta JE, Chen Y, Whitehead EH, Guimaraes C, Panning B, Ploegh HL, Bassik MC, et al. (2014). Genome-Scale CRISPR-Mediated Control of Gene Repression and Activation. Cell 159, 647–661. [PubMed: 25307932]

Hashimoto S, Sugiyama T, Yamazaki R, Nobuta R, and Inada T (2020). Identification of a novel trigger complex that facilitates ribosome-associated quality control in mammalian cells. Sci. Rep 10, 1–12. [PubMed: 31913322]

Horlbeck MA, Gilbert LA, Villalta JE, Adamson B, Pak RA, Chen Y, Fields AP, Park CY, Corn JE, Kampmann M, et al. (2016). Compact and highly active next-generation libraries for CRISPR-mediated gene repression and activation. Elife 5.

Ikeuchi K, Tesina P, Matsuo Y, Sugiyama T, Cheng J, Saeki Y, Tanaka K, Becker T, Beckmann R, and Inada T (2019). Collided ribosomes form a unique structural interface to induce Hel2-driven quality control pathways. EMBO J. 38.

Izawa T, Tsuboi T, Kuroha K, Inada T, Nishikawa S. ichi, and Endo T (2012). Roles of Dom34:Hbs1 in Nonstop Protein Clearance from Translocators for Normal Organelle Protein Influx. Cell Rep. 2, 447–453. [PubMed: 22981232]

Jost M, Santos DA, Saunders RA, Horlbeck MA, Hawkins JS, Scaria SM, Norman TM, Hussmann JA, Liem CR, Gross CA, et al. (2020). Titrating gene expression using libraries of systematically attenuated CRISPR guide RNAs. Nat. Biotechnol 38, 355–364. [PubMed: 31932729]

Juszkiewicz S, and Hegde RS (2017). Initiation of Quality Control during Poly(A) Translation Requires Site-Specific Ribosome Ubiquitination. Mol. Cell 65, 743–750.e4. [PubMed: 28065601]

Juszkiewicz S, Chandrasekaran V, Lin Z, Kraatz S, Ramakrishnan V, and Hegde RS (2018). ZNF598 Is a Quality Control Sensor of Collided Ribosomes Correspondence. Mol. Cell 72, 469–481. [PubMed: 30293783]

Klauer AA, and van Hoof A (2012). Degradation of mRNAs that lack a stop codon: A decade of nonstop progress. Wiley Interdiscip. Rev. RNA 3, 649–660. [PubMed: 22740367]

Kostova KK, Hickey KL, Osuna BA, Hussmann JA, Frost A, Weinberg DE, and Weissman JS (2017). CAT-tailing as a fail-safe mechanism for efficient degradation of stalled nascent polypeptides. Science (80-.). 357.

Krumm N, Turner TN, Baker C, Vives L, Mohajeri K, Witherspoon K, Raja A, Coe BP, Stessman HA, He Z-X, et al. (2015). Excess of rare, inherited truncating mutations in autism. Nat. Genet 47, 582–588. [PubMed: 25961944]

Kryszke M-H, Adjeriou B, Liang F, Chen H, and Dautry F (2016). Post-transcriptional gene silencing activity of human GIGYF2.

Letzring DP, Wolf AS, Brule CE, and Grayhack EJ (2013). Translation of CGA codon repeats in yeast involves quality control components and ribosomal protein L1. Rna 19, 1208–1217. [PubMed: 23825054]

Lytvynenko I, Paternoga H, Thrun A, Balke A, Müller TA, Chiang CH, Nagler K, Tsaprailis G, Anders S, Bischofs I, et al. (2019). Alanine Tails Signal Proteolysis in Bacterial Ribosome-Associated Quality Control. Cell 178, 76–90.e22. [PubMed: 31155236]

Matsuo Y, Ikeuchi K, Saeki Y, Iwasaki S, Schmidt C, Udagawa T, Sato F, Tsuchiya H, Becker T, Tanaka K, et al. (2017). Ubiquitination of stalled ribosome triggers ribosome-associated quality control. Nat. Commun 8, 159. [PubMed: 28757607]

McGlincy NJ, and Ingolia NT (2017). Transcriptome-wide measurement of translation by ribosome profiling. Methods 126, 112–129. [PubMed: 28579404]

Moon SL, Morisaki T, Stasevich TJ, and Parker R (2020). Coupling of translation quality control and mRNA targeting to stress granules. 10.1101/2020.01.05.895342.

Morita M, Ler LW, Fabian MR, Siddiqui N, Mullin M, Henderson VC, Alain T, Fonseca BD, Karashchuk G, Bennett CF, et al. (2012). A Novel 4EHP-GIGYF2 Translational Repressor Complex Is Essential for Mammalian Development. Mol. Cell. Biol 32, 3585–3593. [PubMed: 22751931]

Osuna BA, Howard CJ, KC S, Frost A, and Weinberg DE (2017). In vitro analysis of RQC activities provides insights into the mechanism and function of CAT tailing. Elife 6.

Ozgur S, Chekulaeva M, and Stoecklin G (2010). Human Pat1b Connects Deadenylation with mRNA Decapping and Controls the Assembly of Processing Bodies. Mol. Cell. Biol 30, 4308–4323. [PubMed: 20584987]

Peter D, Weber R, Sandmeir F, Wohlbold L, Helms S, Bawankar P, Valkov E, Igreja C, and Izaurralde E (2017). GIGYF1/2 proteins use auxiliary sequences to selectively bind to 4EHP and repress target mRNA expression. Genes Dev. 31.

Qi LS, Larson MH, Gilbert LA, Doudna JA, Weissman JS, Arkin AP, and Lim WA (2013). Repurposing CRISPR as an RNA-guided platform for sequence-specific control of gene expression. Cell 152, 1173–1183. [PubMed: 23452860]

Ran FA, Hsu PD, Wright J, Agarwala V, Scott DA, and Zhang F (2013). Genome engineering using the CRISPR-Cas9 system. Nat. Protoc 8, 2281–2308. [PubMed: 24157548]

Rom E, Kim HC, Gingras AC, Marcotrigiano J, Favre D, Olsen H, Burley SK, and Sonenberg N (1998). Cloning and characterization of 4EHP, a novel mammalian eIF4E-related cap-binding protein. J. Biol. Chem 273, 13104–13109. [PubMed: 9582349]

Rothstein R (1991). Targeting, Disruption, Replacement, and Allele Rescue: Integrative DNA Transformation in Yeast. Methods Enzymol. 194, 281–301. [PubMed: 2005793]

Saito K, Horikawa W, and Ito K (2015). Inhibiting K63 Polyubiquitination Abolishes No-Go Type Stalled Translation Surveillance in Saccharomyces cerevisiae. PLOS Genet. 11, e1005197. [PubMed: 25909477]

Shao S, and Hegde RS (2014). Reconstitution of a Minimal Ribosome-Associated Ubiquitination Pathway with Purified Factors. Mol. Cell 55, 880–890. [PubMed: 25132172]

Shao S, Von der Malsburg K, and Hegde RS (2013). Listerin-dependent nascent protein ubiquitination relies on ribosome subunit dissociation. Mol. Cell 50, 637–648. [PubMed: 23685075]

Shao S, Brown A, Santhanam B, and Hegde RS (2015). Structure and Assembly Pathway of the Ribosome Quality Control Complex. Mol. Cell 57, 433–444. [PubMed: 25578875]

Sheu-Gruttadauria J, and MacRae IJ (2018). Phase Transitions in the Assembly and Function of Human miRISC. Cell 173, 946–957.e16. [PubMed: 29576456]

Simms CL, Yan LL, Correspondence HSZ, and Zaher HS (2017). Ribosome Collision Is Critical for Quality Control during No-Go Decay Article Ribosome Collision Is Critical for Quality Control during No-Go Decay. Mol. Cell 68, 361–373. [PubMed: 28943311]

Sundaramoorthy E, Leonard M, Mak R, Liao J, Fulzele A, and Bennett EJ (2017). ZNF598 and RACK1 Regulate Mammalian Ribosome-Associated Quality Control Function by Mediating Regulatory 40S Ribosomal Ubiquitylation. Mol. Cell 65, 751–760.e4. [PubMed: 28132843]

Thyme SB, Pieper LM, Li EH, Pandey S, Wang Y, Morris NS, Sha C, Choi JW, Herrera KJ, Soucy ER, et al. (2019). Phenotypic Landscape of Schizophrenia-Associated Genes Defines Candidates and Their Shared Functions. Cell 177, 478–491.e20. [PubMed: 30929901]

Tollenaere MAX, Tiedje C, Rasmussen S, Nielsen JC, Vind AC, Blasius M, Batth TS, Mailand N, Olsen JV, Gaestel M, et al. (2019). GIGYF1/2-Driven Cooperation between ZNF598 and TTP in Posttranscriptional Regulation of Inflammatory Signaling. Cell Rep. 26, 3511–3521.e4. [PubMed: 30917308]

Tyanova S, Temu T, Sinitcyn P, Carlson A, Hein MY, Geiger T, Mann M, and Cox J (2016). The Perseus computational platform for comprehensive analysis of (prote)omics data. Nat. Methods 13, 731–740. [PubMed: 27348712]

Verma R, Oania RS, Kolawa NJ, and Deshaies RJ (2013). Cdc48/p97 promotes degradation of aberrant nascent polypeptides bound to the ribosome. Elife 2, e00308. [PubMed: 23358411]

Wilusz JE, JnBaptiste CK, Lu LY, Kuhn C-D, Joshua-Tor L, and Sharp PA (2012). A triple helix stabilizes the 3’ ends of long noncoding RNAs that lack poly(A) tails. Genes Dev. 26, 2392–2407. [PubMed: 23073843]

Yonashiro R, Tahara EB, Bengtson MH, Khokhrina M, Lorenz H, Chen KC, Kigoshi-Tansho Y, Savas JN, Yates JR, Kay SA, et al. (2016). The Rqc2/Tae2 subunit of the ribosome-associated quality control (RQC) complex marks ribosome-stalled nascent polypeptide chains for aggregation. Elife 5.

Zuberek J, Kubacka D, Jablonowska A, Jemielity J, Stepinski J, Sonenberg N, and Darzynkiewicz E (2007). Weak binding affinity of human 4EHP for mRNA cap analogs. 13, 691–697.

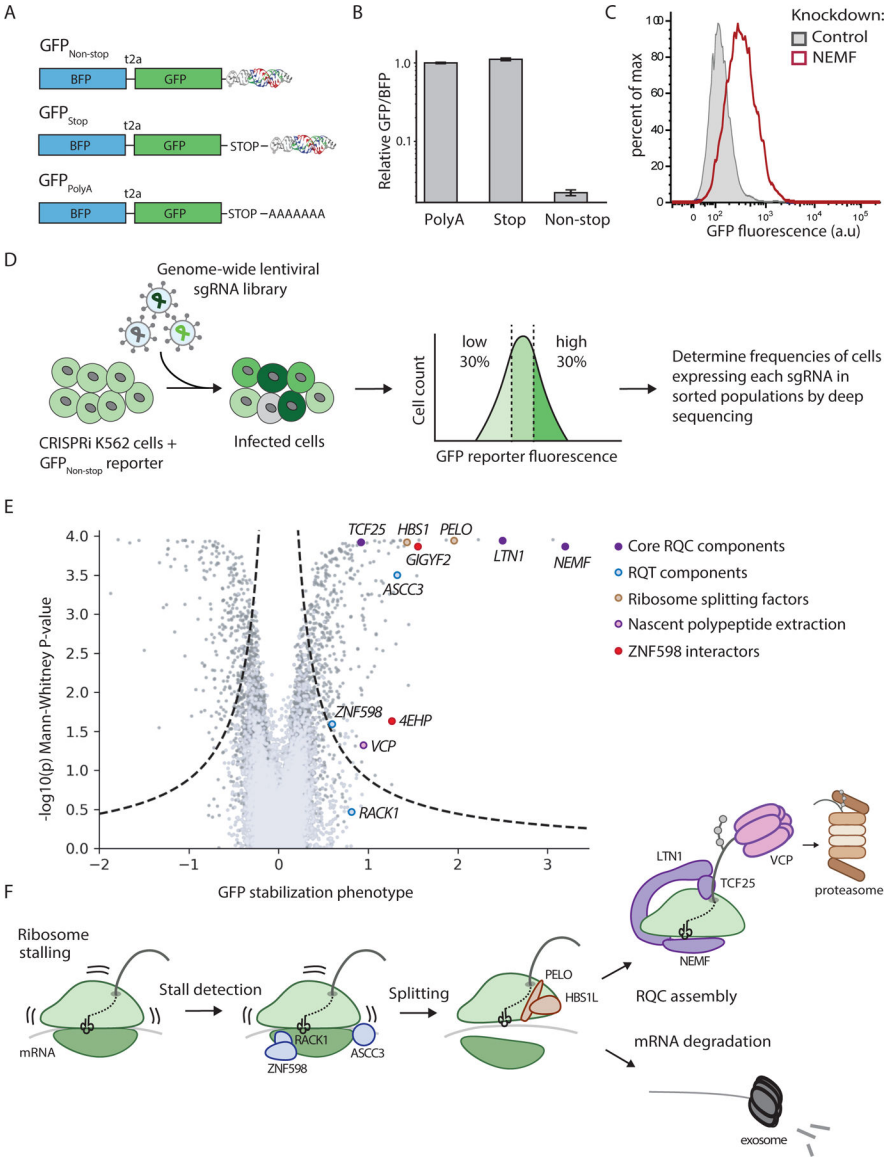

Fig. 1. Genome-wide CRISPRi screen for mammalian RQC components.

(**A**) Diagrams of non-stop stalling reporter ($GFP_{Non\text{-}stop}$) and control reporters (GFP_{Stop} and GFP_{polyA}) (**B**) Median GFP:BFP ratio of 293T cells transiently transfected with reporter constructs containing the indicated 3' mRNA sequence (median ± SD, N=3). (**C**) GFP fluorescence level in cell lines stably expressing the $GFP_{Non\text{-}stop}$ reporter and control sgRNA or sgRNA against *NEMF*. (**D**) Workflow of FACS-based CRISPRi screen. Reporter cell line constitutively expressing $GFP_{Non\text{-}stop}$ is infected with the whole genome CRISPRi sgRNA library. Knockdown of genes involved in coping with ribosome stalling leads to GFP accumulation. GFP-positive and GFP-negative cells are sorted out and the sgRNAs expressed in those cells are identified via deep sequencing. (**E**) Volcano plot of GFP stabilization phenotype (log_2(GFP high/GFP low) for 3 strongest sgRNAs) and Mann-Whitney P-values from genome-scale CRISPRi FACS screen. Negative controls are shown

in lavender, targeting guides in grey, and previously characterized RQC factors are labeled with unique colors. (**F**) Model of the mammalian RQC pathway with screen hits highlighted.

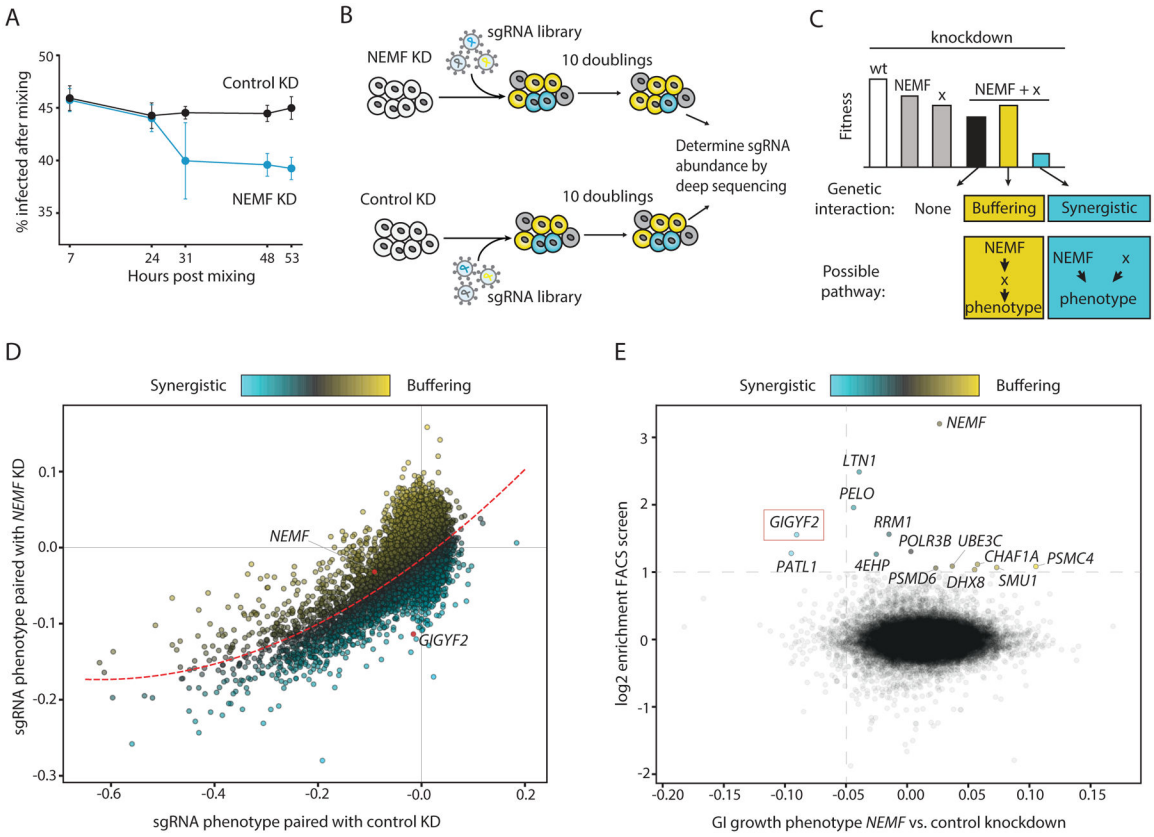

Fig. 2. CRISPRi genetic interaction screen for factors that affect the growth of NEMF knockdown cells.

(**A**) Competition assay between cells expressing a control or NEMF targeting sgRNA. (B) Workflow of growth-based CRISPRi screen. Control knockdown or NEMF knockdown cell lines were infected with the genome-scale sgRNA library and the change in the sgRNA abundance between the two cell lines following 10 cell doublings was determined by deep sequencing. (**C**) Expected growth phenotypes and predicted biological pathways resulting from knockdown of a hypothetical factor (X) alone or in combination with NEMF. (D) Results from genetic interaction (GI) screen for factors affecting the growth of control or *NEMF* knockdown cells. GI scores were derived by fitting the data to a quadratic curve (red dashed line) and calculating the distance of each point from the best-fit line. Genes exhibiting synergistic interactions with *NEMF* knockdown vs. control knockdown (negative GI score) are marked in blue, and genes with positive GI score (buffering interactions) are in yellow. (**E**) Comparison of FACS and GI CRISPRi screens. Hits from FACS screen (log2 enrichment > 1) that stabilized $GFP_{non\text{-}stop}$ reporter upon individual re-testing are labeled and colored by GI score.

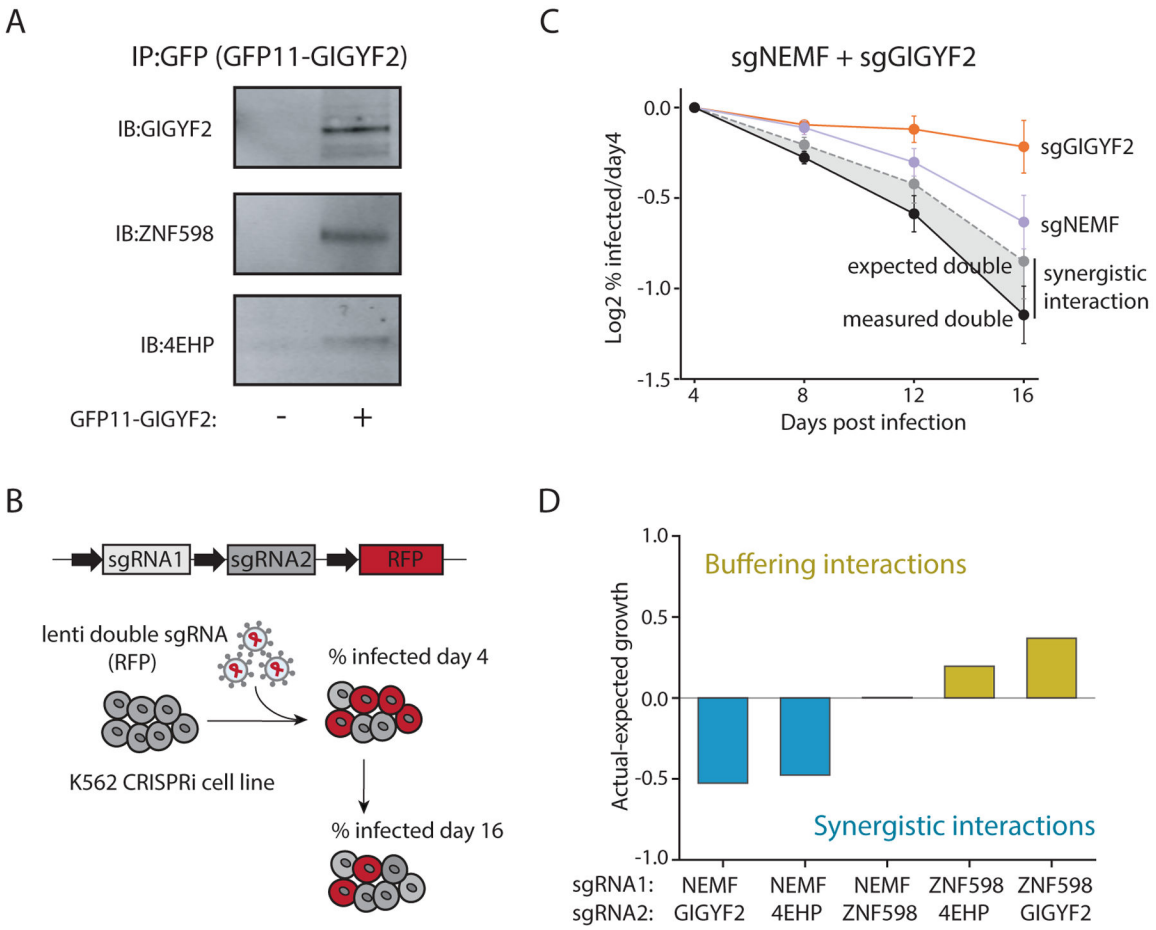

Fig. 3. GIGFY2 and 4EHP are components of a pathway parallel to the RQC.

(**A**) Immunoprecipitation (IP) and immunoblot (IB) for endogenously tagged GIGYF2, and its binding partners, ZNF598 and 4EHP. (**B**) Outline of growth competition experiments. K562 cells were infected with RFP labeled construct carrying two sgRNAs (targeting + control or two targeting guides). The abundance of RFP positive cells is measured over time via flow cytometry. (**C**) Competition assay among cells expressing sgRNA targeting GIGYF2 and NEMF alone or in combination (mean ± SD, N=2). Dotted grey line highlights the expected growth phenotype and the black line represents the observed growth defect of the double knockdown cells. The deviation from the expected phenotype is indicative of synergistic growth interaction. (**D**) Competition assay of double knockdown cell lines. The bar graph represents the difference in the measured (actual) growth defect and expected phenotype (additive value of single growth defects) on day 16 of the competition assay.

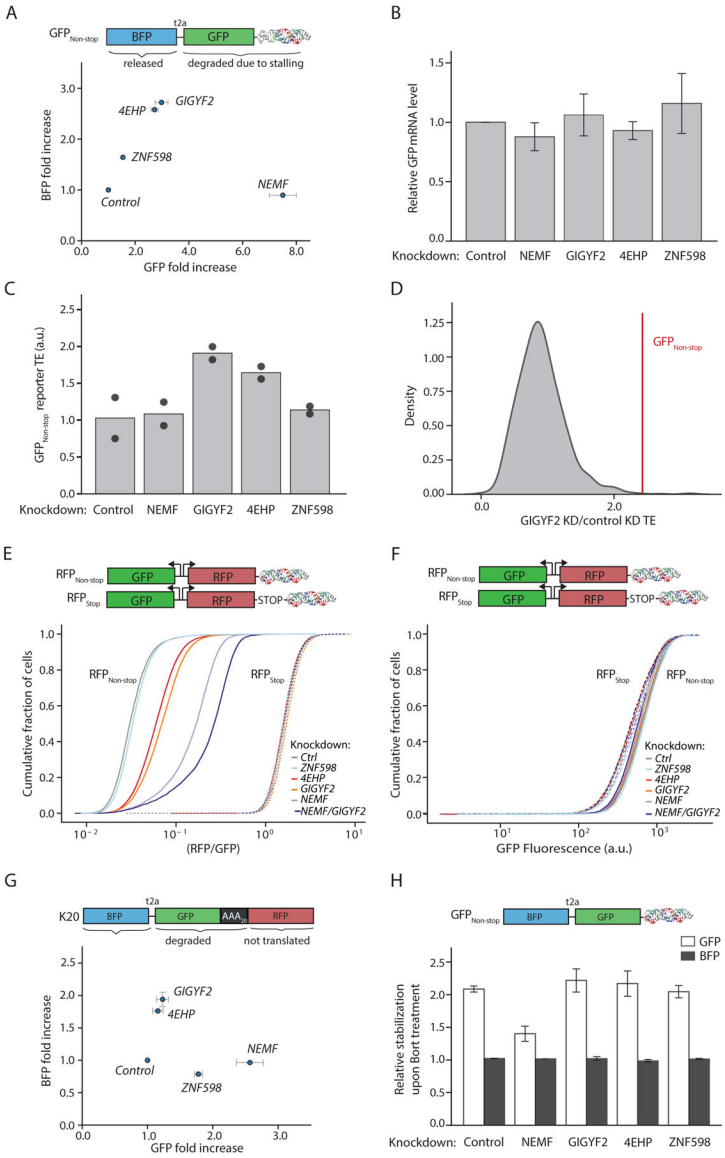

Fig. 4. GIGYF2 and 4EHP selectively inhibit translation of faulty messages harboring stalled ribosomes.

(A) BFP and GFP fold change upon knockdown of various RQC factors measured by flow cytometry (median ± SD, N=3). **(B)** Relative $GFP_{Non\text{-}stop}$ reporter mRNA levels measured by qPCR upon RQC factors knockdown (mean ± SD, N=3). (**C**) Translation efficiency (TE) of GFP non-stop reporter in knockdown cell (bar plot represents the mean, with data points shown, N=2). (**D**) Histogram of TE change in GIGYF2 knockdown compared to control. $GFP_{Non\text{-}stop}$ reporter is highlighted with a red line. (**E**) Bidirectional promoters were used to express GFP with stop codon and polyA tail, and RFP with or without stop codon (diagramed above). Cumulative distribution plot of RFP/GFP protein ratios measured by flow cytometry in RQC knockdown cells lines. Cells expressing $RFP_{Non\text{-}stop}$ reporters are shown as solid lines, whereas cells harboring RFP_{stop} are shown as dashed lines. (**F**) Cumulative distribution plot of GFP protein levels measured by flow cytometry in RQC knockdown cells lines. Solid and dashed lines represent GFP signal from reporter also

containing $RFP_{Non\text{-}stop}$ or RFP_{stop} respectively. **(G)** BFP and GFP protein fold change of K20 stalling reporter upon RQC factors knockdown (median ± SD, N=2). (**H**) Cells expressing $GFP_{Non\text{-}stop}$ reporter were treated with the proteasome inhibitor Bortezomib for 3h and the BFP and GFP protein stabilization was measured by flow cytometry (median ± SD, N=2).

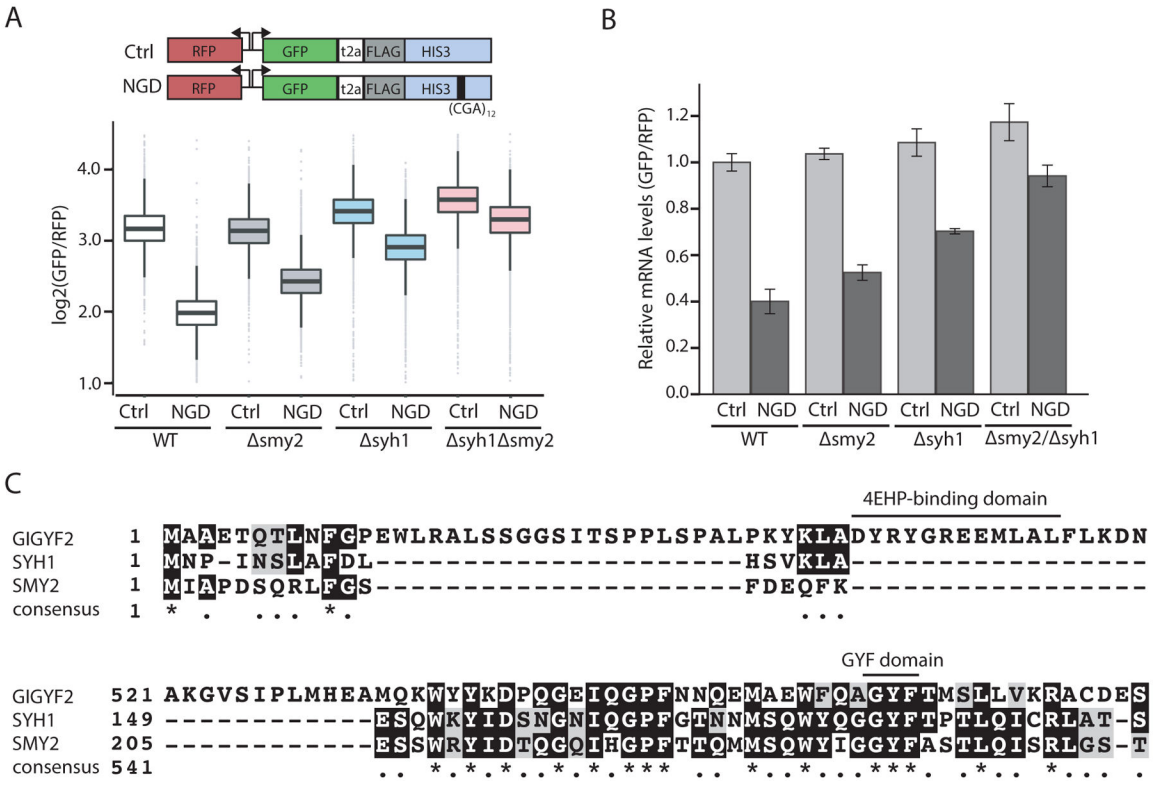

Fig. 5. The yeast homologs of GIGYF2, Smy2p and Syh1p, are RQC factors.

(A) Schematic of control (ctr) reporter and no-go decay (NGD) reporter containing a stretch of 12 non-optimal CGA codons in the middle of the *HIS3* open reading frame (top). Box plot of GFP/RFP ratios for NGD or control reporter levels in knockout yeast strains measured by flow cytometry (bottom). (**B**) Relative mRNA levels for ctr or NGD reporter in wild type or knockout strains measured by qPCR (mean ± SD, N=3). (**C**) Alignment of regions of GIGYF2, Syh1p, and Smy2p highlighting the 4EHP-binding and GYF domains.

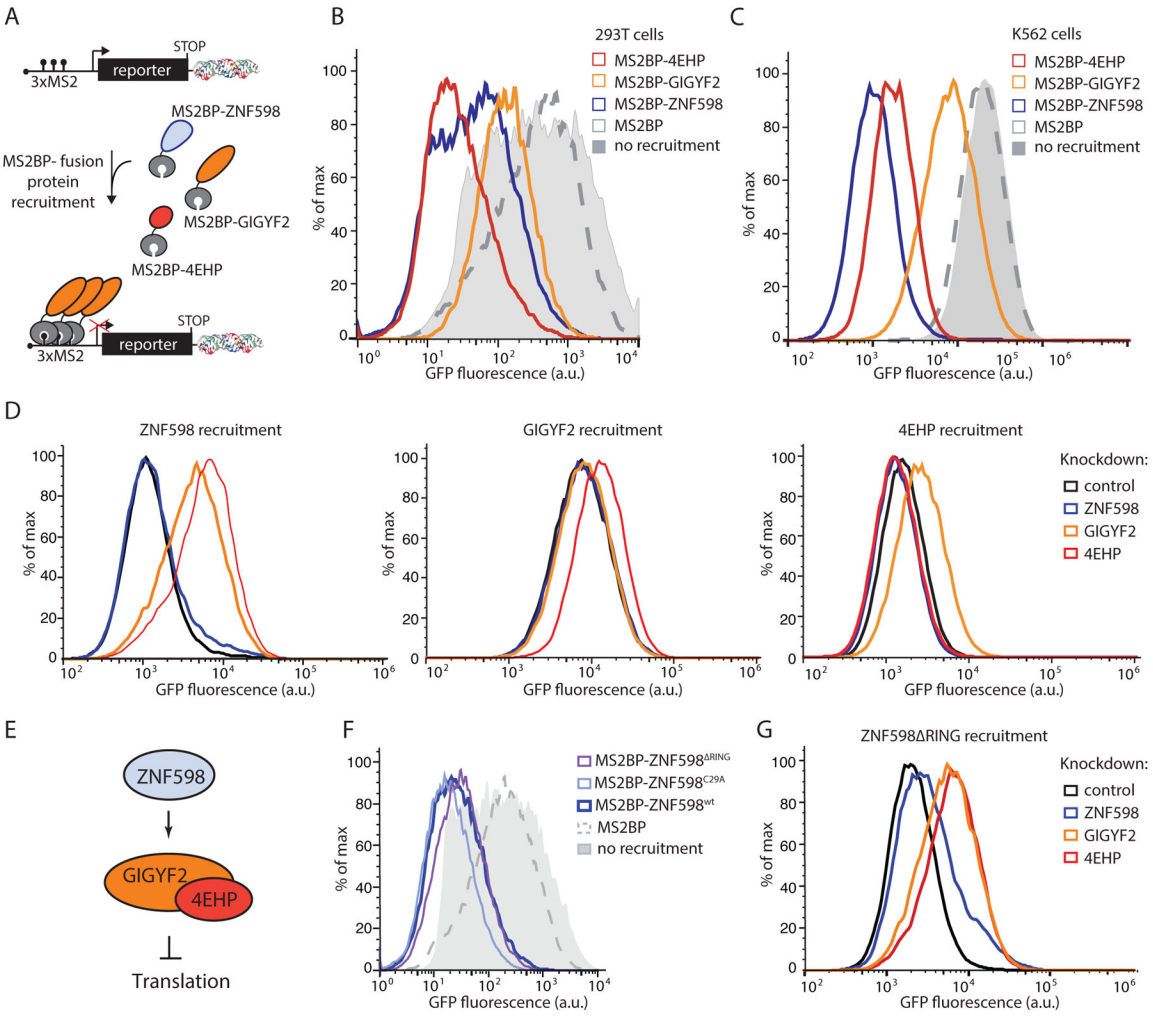

Fig. 6. Translational inhibition by ZNF598 is mediated through GIGYF2 and 4EHP in a ubiquitination-independent manner.

(**A**) Schematic of MS2-mediated recruitment of putative silencing factors to a fluorescent reporter. (**B**) GFP fluorescence of $GFP_{MS2\text{-}stop}$ reporter transiently expressed in HEK293T cells alone or with MS2BP-fusion proteins. (**C**) GFP fluorescence of K562 cells stably expressing $GFP_{MS2\text{-}stop}$ reporter alone or in combination with MS2BP-fusion proteins. (**D, G**) MS2-fusion protein is recruited to the $GFP_{MS2\text{-}stop}$ reporter in control cells or knockdown cells for ZNF598, GIGYF2 or 4EHP. The effect of the knockdown on the ability of the fusion protein to silence translation from the reporter is measured via the change in GFP fluorescence. (**E**) Model for GIGYF2 and 4EHP recruitment to mRNA by ZNF598. (**F**) GFP fluorescence from $GFP_{MS2\text{-}stop}$ reporter upon MS2-mediated recruitment of wild type or ubiquitination incompetent ZNF598 ($ZNF598^{C29A}$ or $ZNF598^{\Delta RING}$).

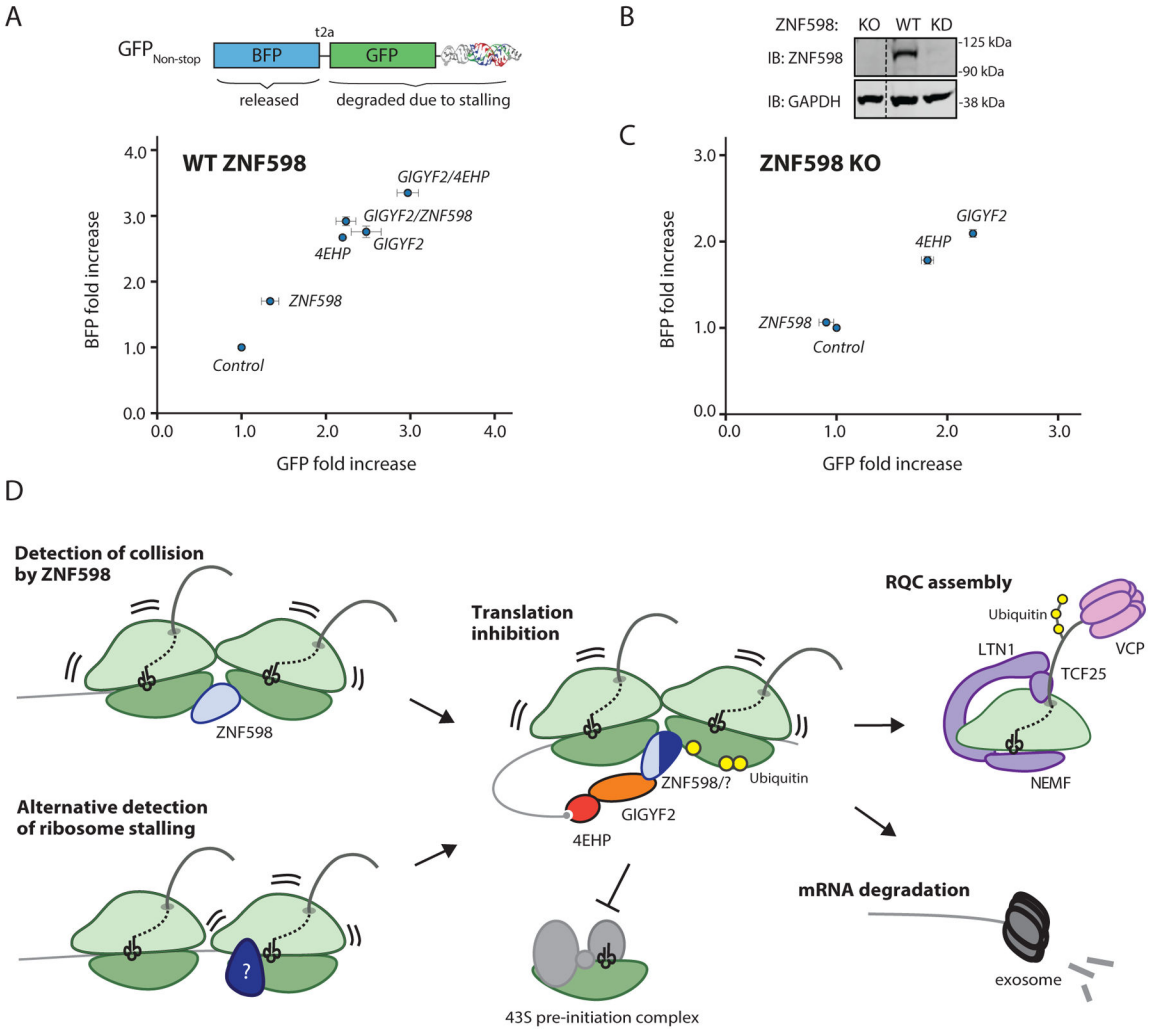

Fig. 7. ZNF598-dependent and independent pathways for GIGYF2–4EHP recruitment and Ribosome-associated Quality Control.

(**A**) BFP and GFP fold change upon single or double RQC factors knockdown measured by flow cytometry (median ± SD, N=2). (**B**) Immunoblot (IB) of ZNF598 in wildtype, ZNF598 knockdown, and ZNF598 knockout cell lines. (**C**) BFP and GFP fold change upon RQC factors knockdown in a ZNF598 knockout cell line measured by flow cytometry (median ± SD, N=2). (**D**) Ribosome collision is detected by the collision sensor ZNF598. Its binding triggers a cascade of events that ultimately leads to the release of the stalled ribosome, and the degradation of the faulty mRNA and stalled nascent peptide. In addition, ZNF598 recruits the translation inhibitors GIGYF2 and 4EHP to the defective message, which blocks further ribosome initiation. Recruitment of GIGYF2 and 4EHP to defective messages could be mediated by factors other than ZNF598.

KEY RESOURCES TABLE

REAGENT or RESOURCE	SOURCE	IDENTIFIER
Antibodies		
Mouse monoclonal [6C5] to GAPDH	Abcam	ab8245
Rabbit anti-ZNF598 Polyclonal Antibody	Bethyl Laboratories, Inc.	A305–108A
rabbit anti-4EHP antibody	Cell Signaling	6916S
rabbit anti-GIGYF2 antibody	Bethyl Laboratories	A303–731A-M
Chemicals, Peptides, and Recombinant Proteins		
Cycloheximide	Sigma-Aldrich	C4859–1ML
Bortezomib	Cell Signaling	#2204
Deposited Data		
CRISPRi FACS screen gene-level table	This study	Table S4
CRISPRi GI screen gene-level table	This study	Table S5
ZNF598 IP-MS data	This study	Table S6
Full Western blot images	This study, Mendeley Data	http://dx.doi.org/10.17632/j42j59f9hf.1
Ribosome profiling/ RNAseq sequencing data	Gene Expression Omnibus	GSE153597
Mass-spectrometry data	ProteomeXchange	PX019961
Experimental Models: Cell Lines		
K562 CRISPRi	(Gilbert et al., 2014)	N/A
K562 CRISPRi $GFP_{Non\text{-}Stop}$	This study	N/A
K562 CRISPRi GFP_{Stop}	This study	N/A
K562 CRISPRi GFP_{PolyA}	This study	N/A
K562 CRISPRi $RFP_{Non\text{-}Stop}$	This study	N/A
K562 CRISPRi RFP_{Stop}	This study	N/A
K562 CRISPRi sgNEMF- RFP	This study	N/A
K562 CRISPRi sgGAL4- RFP	This study	N/A
K562 CRISPRi K20	This study	N/A
HEK 293T GFP1–10 + GIGYF2–11	This study	N/A
K562 CRISPRi MS2-GFP_{Stop} cell line	This study	N/A
K562 CRISPRi $GFP_{Non\text{-}stop}$ ZNF598 knockout	This study	N/A
Experimental Models: Yeast Strains		
MATa his3Δ1 leu2Δ0 met15Δ0 ura3Δ0 ade2::RFP_Pgal_GFP-2A-FLHIS3_MET17	(D'Orazio et al., 2019)	N/A
MATa his3Δ1 leu2Δ0 met15Δ0 ura3Δ0 ade2::RFP_Pgal_GFP-2A-FLHIS3_CGA12_His3_MET17	(D'Orazio et al., 2019)	N/A
MATa his3Δ1 leu2Δ0 met15Δ0 ura3Δ0 smy2::HygB ade2::RFP_Pgal_GFP-2A-FLHIS3_MET17	This study	N/A
MATa his3Δ1 leu2Δ0 met15Δ0 ura3Δ0 smy2::HygB ade2::RFP_Pgal_GFP-2A-FLHIS3_CGA12_HIS3_MET17	This study	N/A

REAGENT or RESOURCE	SOURCE	IDENTIFIER
MATa his3Δ1 leu2Δ0 met15Δ0 ura3Δ0 syh1::KanMX4 ade2::RFP_Pgal_GFP-2A-FLHIS3_MET17	This study	N/A
MATa his3Δ1 leu2Δ0 met15Δ0 ura3Δ0 syh1::KanMX4 ade2::RFP_Pgal_GFP-2A-FLHIS3_CGA12_HIS3_MET17	This study	N/A
MATa his3Δ1 leu2Δ0 met15Δ0 ura3Δ0 smy2::HygB syh1::KanMX4 ade2::RFP_Pgal_GFP-2A-FLHIS3_MET17	This study	N/A
MATa his3Δ1 leu2Δ0 met15Δ0 ura3Δ0 smy2::HygB syh1::KanMX4 ade2::RFP_Pgal_GFP-2A-FLHIS3_CGA12_HIS3_MET17	This study	N/A
Oligonucleotides		
See Table S3 for qPCR primers	This study	N/A
See Table S2 for protospacer sequences	This study	N/A
Recombinant DNA		
hCRISPRi- v2 library	(Horlbeck et al., 2016)	Addgene, Cat#83969
See Table S1 for plasmids	This study	N/A
pSpCas9(BB)-2A-GFP (PX458)	(Ran et al., 2013)	Addgene Cat#48138
pU6-sgRNA EF1alpha-puro-T2A-RFP	(Jost et al., 2020)	N/A
pU6-sgRNA EF1alpha-puro-T2A-BFP	(Gilbert et al., 2014)	Addgene Cat#60955
Software and Algorithms		
Screen Processing Pipeline	Horlbeck et al., 2016	https://github.com/mhorlbeck/ScreenProcessing
FlowJo 8.8.6	FlowJo	https://www.flowjo.com